PROGRAMMATORISCHE FEDERALE OVERHEIDSDIENST

WETENSCHAPSBELEID

RESEARCH PROGRAMME FOR EARTH OBSERVATION "STEREO"

Partnerships between Industry and Research

ONDERZOEKSCONTRACT

CONTRAT DE RECHERCHE

SR/67/36

PROJECT

Operational Remote sensing Mapping of Estuarine suspended Sediment concentrations (ORMES)

Operationele kartering van suspensiesedimentconcentraties in estuaria door middel van aardobservatie (ORMES)

THE PARTNERSHIP

SCIENTIFIC PARTNER

Vlaamse Instelling voor Technologisch Onderzoek (VITO)

PRIVATE PARTNER

International and Marine Dredging Consultants (IMDC)

PROGRESS REPORT #3

Covering the period from 15/01/2006 to 15/07/2006

TABLE OF CONTENT

LIST OF TABLES

LIST OF FIGURES

ACRONYMS AND ABBREVIATIONS

AHS	Advanced Hyperspectral Scanner
ASD	Analytical Spectral Devices
CDOM	Color Dissolved Organic Matter
CHL	Chlorophyll
GER	Gaia Environmental Research
GMT	Greenwich Mean Time
HRV	High Resolution Visible
HW	High water
L	At-sensor radiance
L(X)	At sensor radiance at wavelength X
LOOCV	Leave-One-Out cross-Validation
μ	mean
NIR	Near Infrared
R(652)	Reflectance at 652 nm
R(0-)	Subsurface irradiance reflectance
R(0-,X)	Subsurface irradiance reflectance at wavelength X
R^2	Coefficient of determination
s	Standard deviation
RMSE	Root mean square error
SIOP	Specific Inherent Optical Properties
SPM	Suspended Particulate Matter
SPOT	Système Pour l'Observation de la Terre
TM7	Thematic Mapper band 7
TSM	Total Suspended Matter
UTC	Universal Time Coordinated

1. Activity report for the partnership

1.1 Summary

The activity report of the ORMES project describes the scientific progress made during a six month period and the scientific plans for the next six months. The status of the work packages and corresponding deliverables is illustrated in Table 1.

Table 1: ORMES deliverable status

	2005 01-Dec	2006 01-July	2006 07-Dec
WP 0 Project management			
0.1 Coordination	C	C	C
0.2 Organization meetings	C	C	C
0.3 Diffusion valorization	C	C	C
0.4 Reports			
WP 1 Reviewing	D		
WP 2 Campaign preparation			
2.1 Specifications	D		
2.2 Subcontracting flight agency	D		
2.3 Deployment spectrometers	D		
2.4 Transport model optimizing		B	P
WP 3 Campaign			
3.1 Atmospheric measurements	D		
3.2 Reflectance measurements	D		
3.3 Turbidity measurements	D		
3.4 Water samples	D		
WP 4 Processing field data			
4.1 Laboratory analysis	D		
4.2 Conversion turbidity	D		
WP 5 Processing image data			
5.1 pre-processing	D		
5.2 Applying algorithms		D	
5.3 Accuracy assessment		D	
5.4 determination min. sample size		D	
WP 6 Exporting methodology		B	P
WP 7 Validation		B	P
WP 8 Implementation			
8.1 Specification software		D	
8.2 Development of software		B	P
8.3 Implementation			P

D: Delivered, B: Busy as planned, P: Planned delivery, C: Continuous activity

1.2 Scientific progress, activities and results

1.1.1 Work Package 0 – Project Management

- A steering committee meeting took place on 25 February 2006.
- A paper has been submitted for the proceedings of the International Hydrographic Conference 2006 in Antwerp and has been accepted for oral presentation.
- A paper has been submitted for the proceedings of the International Dredging Days 2006, Tangiers, Morocco and has been accepted for oral presentation.
- A paper has been submitted for Marine Geodesy Journal

1.1.2 Work Package 4 – Processing field data

Histograms are constructed for the Scheldt and the docks to have a better understanding of the distributions of the SPM and CHL concentrations.

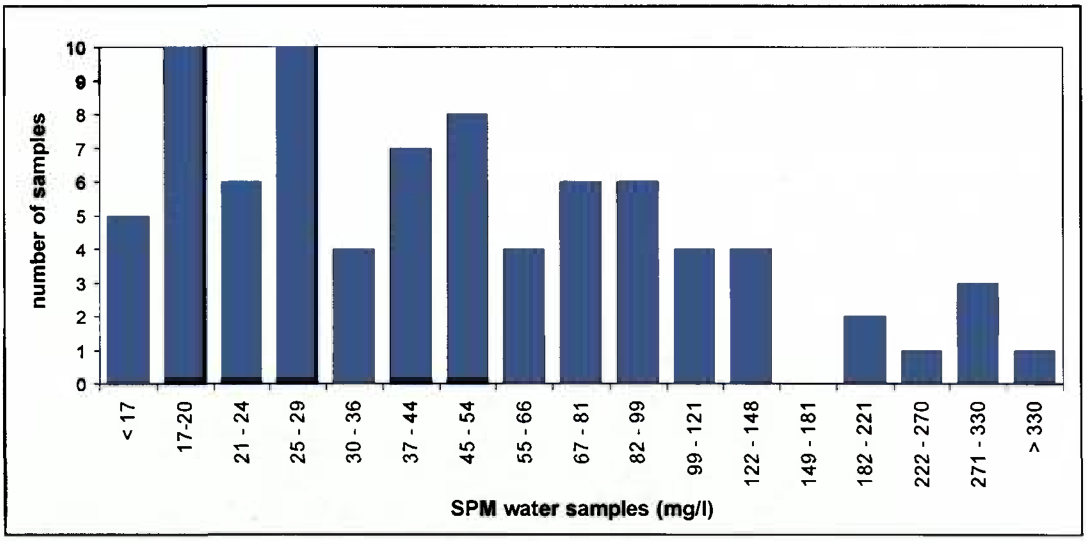

Figure 1: Histogram of the SPM concentrations in the Scheldt

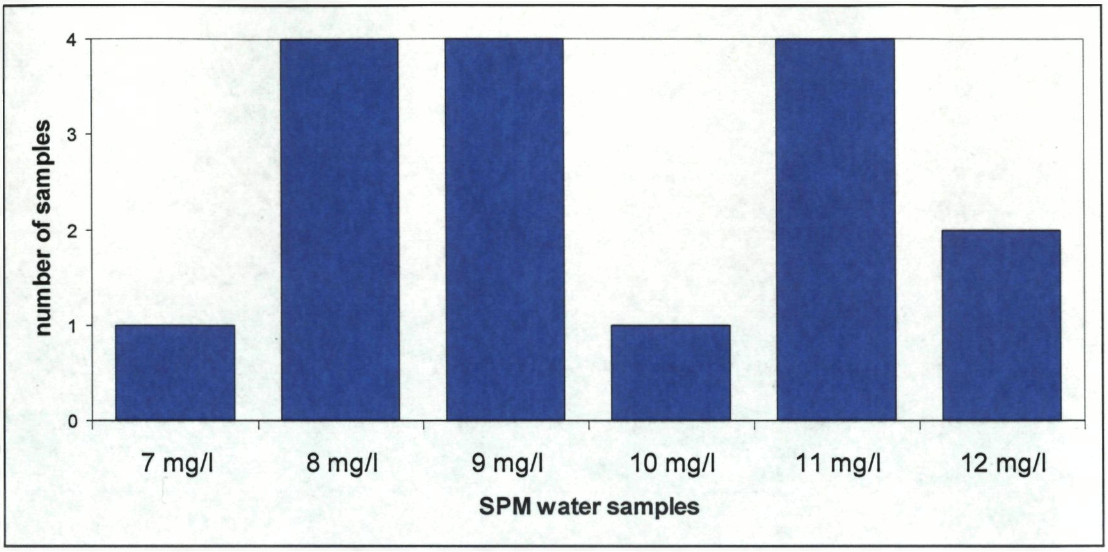

Figure 2: Histogram of SPM concentrations in the docks

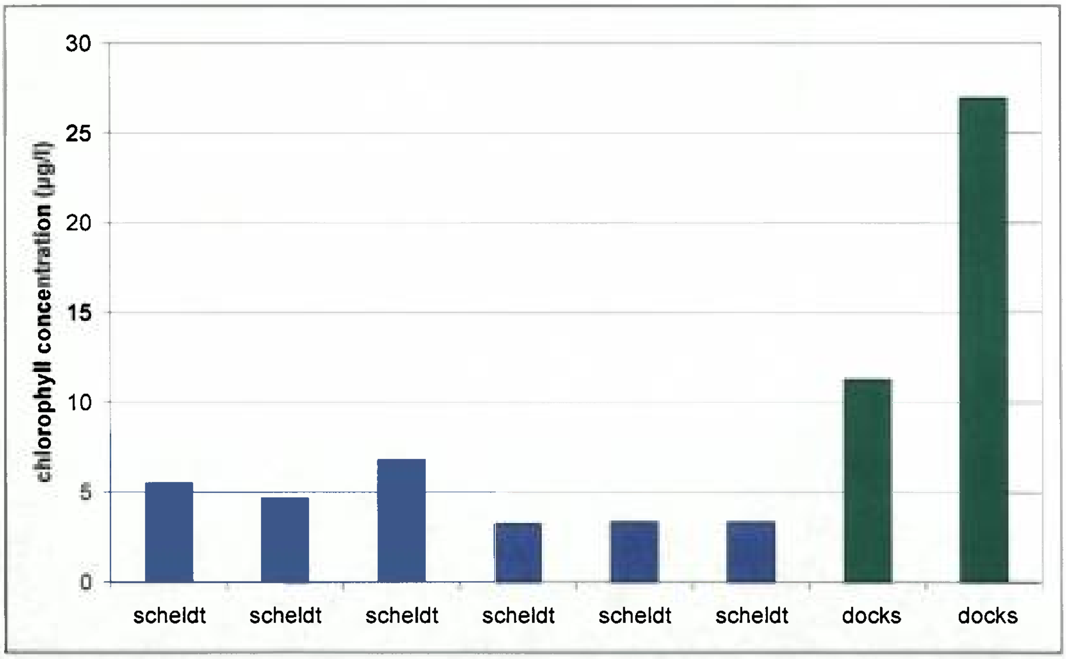

Figure 3: Histogram of chlorophyll concentrations in the docks and in the Scheldt

More details of the field data processing was given in previous report.

1.1.3 Work Package 5 – Processing image data

For readers without remote sensing background we would like to refer to ANNEX 2 for a short introduction in remote sensing in order to better understand next paragraphs.

1.1.3.1 Pre-processing

Details of the pre-processing steps can be found in the previous reports.

1.1.3.2 Applying algorithms

Algorithms to retrieve suspended matter (SPM) concentration from remote sensing data can be divided in two broad categories : semi-empirical approaches and analytical models. In table 2 the (dis-)advantages of both methods are listed.

Table 2: (dis-)advantages of semi-empirical and analytical approach

	SEMI-EMPIRICAL	ANALYTICAL MODELS
Approach	Statistical using some physical knowledge	Physical model
Advantages	+ fast + easy to apply	+ model applicable to other regions- + simultaneous determination of different water parameters (CHL, CDOM, SPM)
Disadvantages	- several in-situ measurements of SPM simultaneously with image acquisition required - difficult to apply to other regions without in-situ measurements	- absorption and scattering properties of the area of interest should be known - very sensitive to errors in input parameters - complex

In the ORMES project we tested both approaches to quantify the SPM concentration on the basis of the AHS airborne data.

Empirical approach

As mentioned in table 2 the empirical approach requires in-situ measurements of SPM made simultaneously with the image acquisition. SPM data are available from direct measurements i.e. water samples and indirect measurements i.e. converted from turbidity measurements. As the accuracy of the latter SPM dataset depends on the fit of the statistical relationship of turbidity versus SPM, it was decided to work at first place with the SPM data derived from the water samples. In the Scheldt, the suspended matter concentrations and patterns change very rapidly as the tide fluctuates. Hence, to calibrate as accurately as possible, only the samples taken within a few minutes of the airborne data recording were included. In total 41 samples were available to find a band combination which best predicts the SPM concentrations.

Sub-surface irradiance reflectance R(0-) spectra were extracted from the hyperspectral images at the sampling locations. An average spectrum calculated from a 5 by 5 box of pixels (corresponding to an area of 20 m by 20m) was preferred to remove random noise (Figure 4).

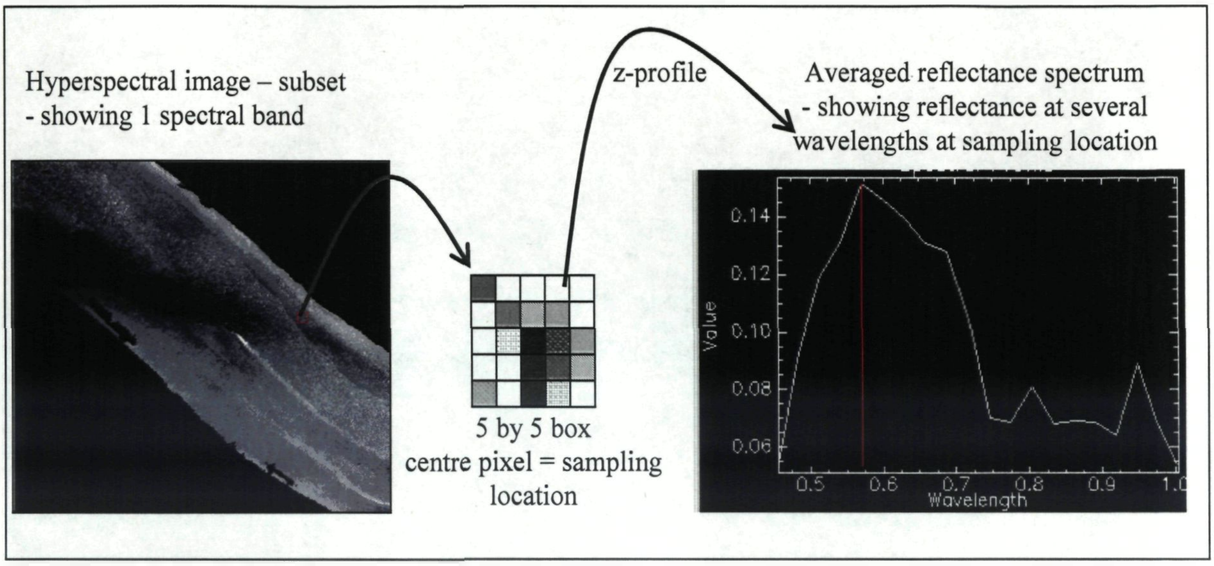

Figure 4: Selection of reflectance spectrum from the hyperspectral image.

Single bands, band ratios, differences of 2 bands were linearly or logarithmically regressed against SPM. Band or band combinations with the highest correlation and minimal root-mean-square-error (RMSE) were judged on their physical relevance.
The best fit with an R^2 of 0.83 and an RMSE of 15.53 mg/l was found to be a log-linear line fit to a band difference (Figure 5):

$$Ln(SPM) = 34.18*(R(0-,833)-R(0-,1004)) + 3.16 \quad [1]$$

where R(0-,833) and R(0-,1004) are respectively the subsurface irradiance reflectance at 833 nm and 1004 nm.

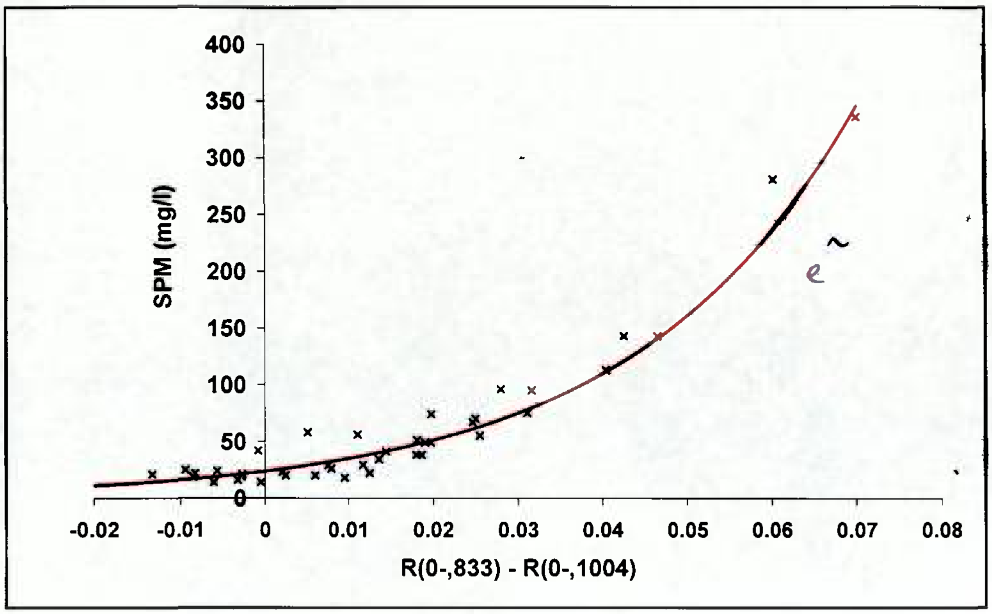

Figure 5: Regression line for algorithm [1]

The use of a difference of two NIR bands can be explained physically: (1) the NIR band is shown to be highly correlated to SPM and (2) the subtraction of the 1004 nm band seems to be correcting for differences in cloud cover and adjacency effects.

The algorithm [1] providing the best fit was then applied to all the AHS data to map SPM concentration at different tidal stages. Figures 6 and 7 show SPM maps for flightline 1 and 4 respectively.

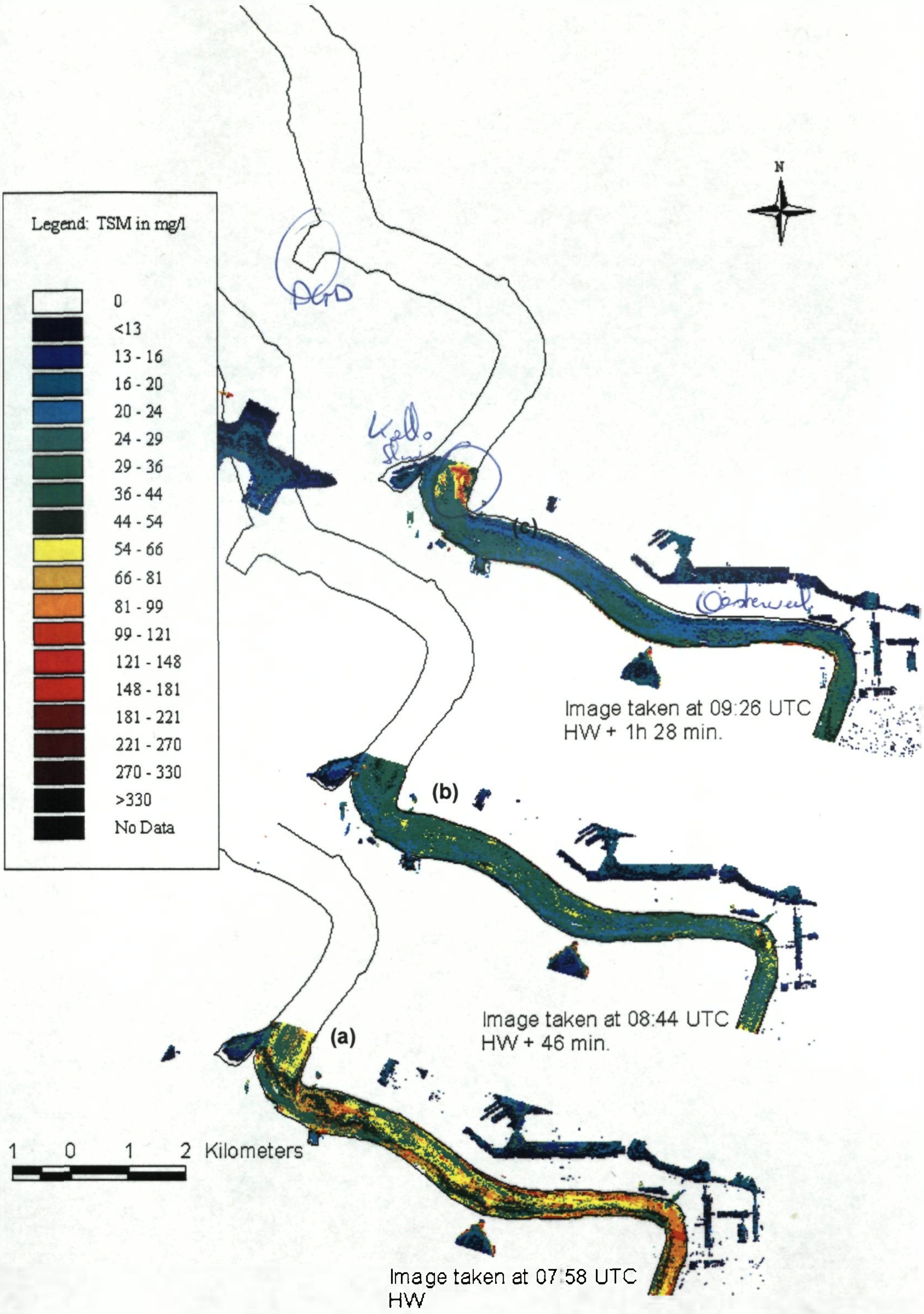

Figure 6: TSM maps of flightline 1

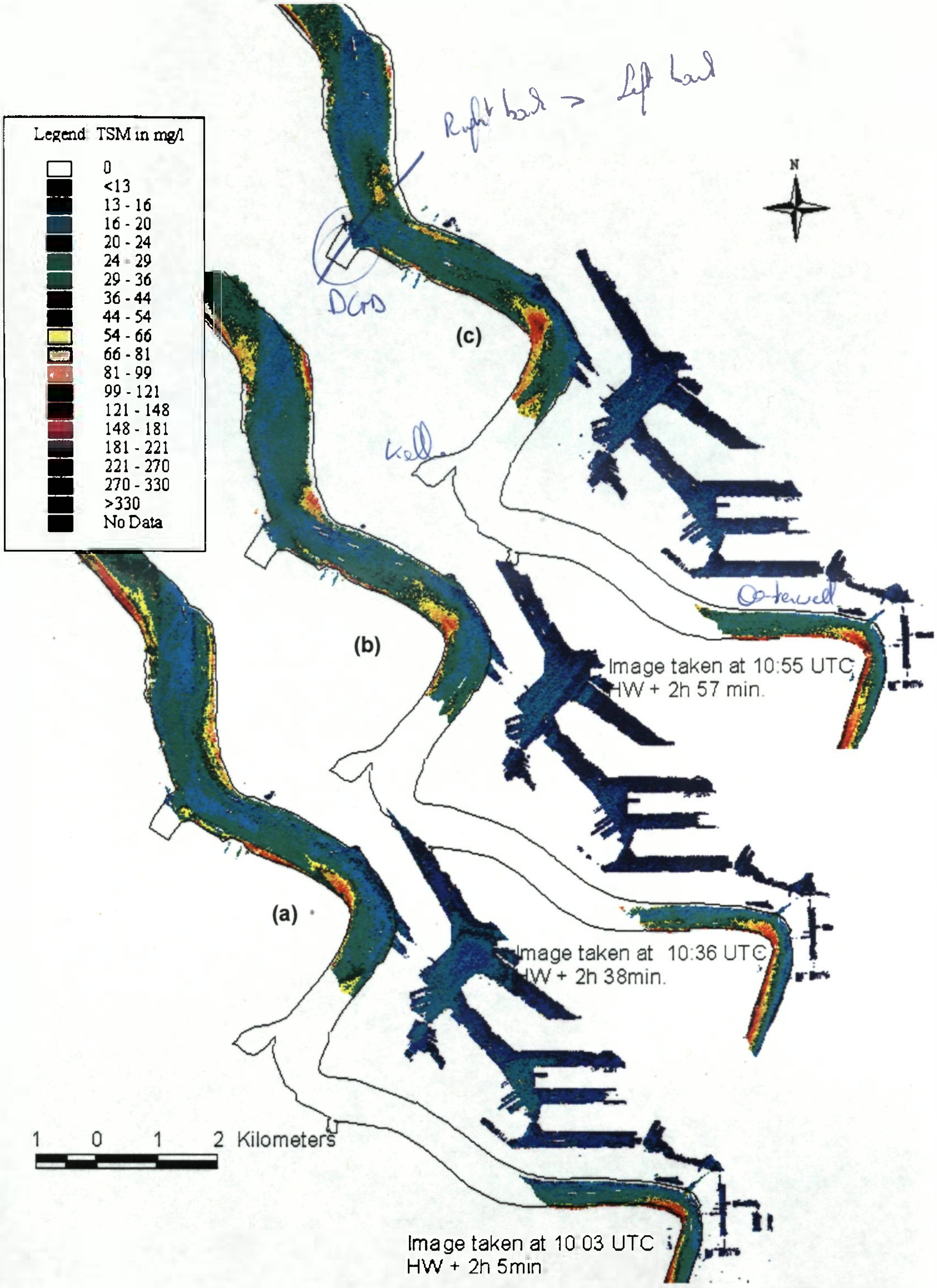

Figure 7: TSM maps of flightline 4

Analytical approach

In the analytical approach the water constituent concentrations are physically related to the measured reflectance spectra using sophisticated radiative transfer or (semi-) analytical bio-optical models. To determine the water quality parameters (e.g. SPM) these models are inverted. This approach requires detailed information about the specific inherent optical properties (SIOP) like the absorption and the backscattering spectra per unit constituent.

Within the ORMES project we tested the analytical models proposed by Gordon et. al. (1988) and by Albert and Mobley (2003). The resulting SPM concentrations were compared to the SPM data retrieved from the water samples. Unfortunately only for a few water samples good results were obtained. For high concentrations the SPM was strongly underestimated. This latter finding is in agreement with the results of Kempeneers et al. (2005). In general we can conclude that analytical approaches are very sensitive to inaccuracies in both the reflectance spectra and SIOP data.

1.1.3.3 Accuracy assessment

Statistical approach

To predict how well the algorithm [1] will perform for the entire dataset a cross-validation is applied. Cross-validation is carried out by splitting the dataset into two parts - one part for training and one part for testing. However, it was preferred here to apply a leave-one-out cross-validation because of the limited number of ground sample calibration points available. Applying the leave-one-out cross-validation (LOOCV), all samples except 1 are used for establishing the calibration relation. By rotating the left-out sample over successive training and validation steps, the possible bias by relying on a single split into training and test samples is avoided. The RMSE of the LOOCV for our log-linear line model was 17.06 mg/l.

Historical data and background knowledge of Scheldt turbidity patterns

The produced sediment maps show good agreement with known variations of turbidity over the tidal cycle: maximum turbidity around high water, gradual settling of the sediment in the succeeding slack water and resuspension at the onset of the ebb flow stage.

Figure 6a, taken at high tide, shows –compared to the other figures – high surface silt concentration. These general high near-surface SPM concentrations are mainly explained by high current velocities at high tide. The high concentrations are spread out over the whole cross-section, similar to the velocity distribution pattern observed by Fettweis et al.

(1998). In the entrance channel of Kallo where velocities are much lower, lower silt concentrations at the surface can be observed.
In the succeeding slack tide high water (Figure 6b) the observed SPM concentrations are much lower. At this stage velocities are very low, which results in much lower surface concentrations of SPM, due to the sinking of the sediment particles (IMDC, 1999, 2004).
A resuspension of sediment takes place at the onset of the ebb flow stage, especially at the bend-related shoals (Figure 6c). During ebb (Figure 7a-c) downstream velocities are observed, i.e. the sediment concentration is higher downstream of the inside of curbs which are shallower areas. Eroded sediment at the shallow area is dragged in the downstream direction. The distribution and concentration of the sediments remain relatively constant during these 3 successive tidal stages (Figure 7a-c). The horizontal cross-section variation in SPM matches the variation measured at previous field campaigns. Surface silt concentrations are higher at the right bank than at the left bank (IMDC, 2005). A striking feature of sediment plume at this stage of the tide is observed at the Doel flow guidance dam, which emerges at low water. The submerged flow guidance dike clearly separates high silt concentrations west of the dike from low silt concentrations east of the dike. This dike is the border between a shallow area (resulting in high sediment concentrations at the surface) west and the navigation channel eastward.
Another known feature, well present in all the produced maps, is the low-SPM concentration in the harbour docks. Some sediment enters the docks near the access locks during sluicing operations. This sediment settles in the adjacent harbour dock. To verify these conclusions extra validation will be performed using a series of turbidity measurements along horizontal cross-section transects made by IMDC in the past at different stages of the tidal cycle.

Through Tide Measurements that occurred in the past at the same locations as the ORMES measurement campaign were used to validate SPM concentration near the water surface. Qualitative comparison of horizontal variation at certain transects, tidal variation at fixed points were investigated to validate the remote sensing images. (ANNEX 8)

1.1.3.4 Determination minimum sample size

Determination of minimum sample sizes for regression analysis depends in high degree on the research question 'What is the main objective of the regression analysis?'. In ANNEX 3 an overview is given of the different approaches to determine sample size in function of the research question.

1.1.4 *Work package 6 – Exporting the methodology*

We ordered SPOT satellite data from the Scheldt. Unfortunately SPOTimage cancelled our image request at the last moment and no SPOT data were acquired. Later on, attempts to acquire SPOT and FORMOSAT images of Botlek harbor failed.

Therefore we had to use simulated SPOT and Landsat data created by spectrally and spatially resampling the AHS data. The results of this approach are given in ANNEX 4.

1.1.5 *Work package 7 – Validation*

A sensitivity analysis is performed to test the robustness of the relationship [1] to uncertainties in the inputs, or more precisely, how RMSE,R^2 and the final SPM maps respond to these uncertainties. A detailed description and results of this sensitivity analysis can also be found in ANNEX 4, chapter 1.

Furthermore we tested if different results would be obtained if no atmospheric and air-interface correction is performed on the data. The results are described in ANNEX 4, chapter 2.

Finally at-sensor radiance spectra, corresponding to large range of SPM and CHL concentrations, were simulated in order to test influence of chlorophyll variation and adjacency effects[1] on the performance of the SPM algorithms. A detailed description and results of this sensitivity analysis can also be found in ANNEX 4,chapter 3 .

1.1 Encountered problems and dead-end tracks

The following problems have been encountered in the ORMES project up till now :

1. Bad weather conditions during AHS airborne campaign: Although weather forecasts were optimistic and the sky was clear at the beginning of the campaign, thin cirrus clouds covered the study area gradually (see ANNEX 5). Around noon it started to rain and the flight lines planned for the afternoon were cancelled. The bad weather conditions and subsequently canceling of the flights entailed the following problems:
   1. Atmospheric correction algorithms are not well adapted to cloudy conditions. Cloud models can be used in the correction process. However due to the strong variability in the cloud thickness and cover the standard cloud models will almost never represent the true atmospheric conditions. *Adopted solution* : *The algorithm [1] derived for SPM mapping contains a difference term sets off two reflectance*

[1] High resolution images acquired from lakes, rivers and coastal areas are influenced by atmospheric adjacency effects Radiance from adjacent areas may be scattered into the field of view of the sensor The adjacency effect reduces the apparent spatial resolution and modifies the spectral signature of the observed pixel (Kaufman,1984) Dark pixels look brighter and bright pixels look darker Increased radiance values of the water pixels might easily be mistaken for bottom effects or suspended sediments

values in the near infrared range, of which one is and the other is not sediment-dependent This strategy showed to compensate for some disturbing factors, such as varying cirrus cloud cover. Indeed, the reflectance at 1004 nm is uncorrelated to SPM concentration since at 1004 nm, the penetration depth of sunlight into the water is almost zero and therefore the reflection by suspended sediments at this wavelength is lower than the Signal to Noise of the sensor. This is also demonstrated by the fact that absolutely no correlation was found between SPM and reflectance at 1004 nm ($R^2 = 0.03$). Furthermore, it is known that variation of optical properties of cirrus clouds is negligible in the 0.4 – 1 µm spectral range.

2. The SPM algorithm derived on the basis of the in-situ shipborne reflectance measurements (with GER and ASD spectroradiometer) could not successfully be applied to the airborne data. As seen in figures 13 and 14 of the previous report this algorithm resulted in too high SPM values in for instance the docks. *Adopted solution: In stead of deriving the algorithm on the basis of the shipborne spectra we decided to use the image spectra itself. As described under 1.2.3.3. and illustrated in the figures 5 and 6 this approach gave much better results.*
3. The flight lines in the afternoon were scheduled in order: 1. to cover more stages of the tidal cycle, 2. to increase the variability in SPM concentration ranges (SPM range is influenced by the tidal cycle) and 3. to increase the number of in-situ measurements that could be done simultaneously with the airborne data acquisition.

2. AHS calibration problems: It was the first time that INTA used the AHS sensor for an operational mission since a period of non-activity due to some system problems. It was noticed only several months after acquisition and data delivery that the radiometric calibration (gain and offsets) was inaccurate. Up on VITO's request INTA recalibrated the AHS sensor and provided us with new gain and offsets. These problems caused a serious delay in the image data processing.
3. No satellite data of Scheldt test site : It was intended to have a SPOT satellite image simultaneously with the airborne and shipborne campaign. Unfortunately due to the poor SPOT constellation at the day of the airborne campaign no SPOT image could be acquired. *Adopted solution : SPOT and Landsat were simulated by resampling spatially and spectrally the AHS data. The results are given in ANNEX 4.*
4. Unsuccessful requests for satellite data of foreign validation sites: There were several attempts to request satellite data (SPOT, Formosat) from foreign validation sites. Unfortunately up till now SPOTimage could not fulfill our request.

5. Very high spatial and temporal variability of SPM in the Scheldt : The fit of SPM algorithms decreased slightly when the time difference between SPM data from water samples and turbid and image data increased. *Adopted solution: Special attention was given to include in the algorithm definition only the samples taken within a few minutes of the airborne data recording*
6. validation using turbidity measurements

   It was not possible to quantitatively compare the SPM output map with the turbidity measurements on a pixel-by pixel basis because the SPM concentrations are extremely variable (cfr. previous paragraph)

1.2 Scientific activities planned for the next six months

- Diffusion of the results at Hydro 2006 and International Dredging Days
- Application of the sediment transport model developed by IMDC to the Scheldt river for the day of the airborne campaign and comparison of the results with the SPM maps derived from the airborne data.
- Finalisation of the SPM software and implementation of the software at the IMDC
- Validation on a foreign test site using multi-spectral satellite data

2. Administrative update to initial report

N/A

ANNEX 1 - ANSWERS ON COMMENTS STEERING COMMITTEE

1. **goede communicatie met de eindgebruiker (IMDC). Het is de mening van de stuurgroep dat de eindgebruiker in deze fase van het project meer een kritisch sturende inbreng dient te krijgen dan nu al het geval is. Daarom wordt het wenselijk geacht dat er in een volgend progress report wordt ingegaan op concrete vragen als hoe goed de resultaten uiteindelijk worden verwacht te zijn (in de zin van een onzekerheidsmarge omheen de geschatte SSC-waarden), en hoe IMDC het eindproduct uiteindelijk wenst te gebruiken (combinatie met satelliet in een eerste verkenning, of gebruik van hi-res vliegtuigbeelden in een verdere fase van het project). Een duidelijke afbakening van het toekomstig gebruik van de software-tool zal dat gebruik in belangrijke mate in de hand werken.**

   IMDC is vooral geïnteresseerd in het gebruik van satellietbeelden voor toepassing van het eindproduct, en de betrouwbaarheid van het eindproduct voor een eerste kwalitatieve analyse van een site bij verschillende omstandigheden (historische of recente analyse), alsook van de betrouwbaarheid bij een combinatie van satellietbeelden gecombineerd met een in situ meetcampagne. Het gebruik van hi-res vliegtuigbeelden is, gezien de hogere kost, meer geschikt voor specifieke projecten waar de nodige middelen beschikbaar zijn om gedetailleerd onderzoek uit te voeren.

   IMDC heeft aan VITO al enkele opmerkingen geformuleerd om het eindproduct af te stemmen voor toekomstig gebruik. Enkele voorbeelden hiervan zijn:

   a. het uitvoeren van tests naar de verlaging van nauwkeurigheid voor het geval minder in situ data beschikbaar zijn

   b. onderzoek naar welke satellieten bruikbaar kunnen zijn, en in welke mate ze bruikbaar zijn om historische data te verkrijgen

   c. voor de uitvoer heeft IMDC de nodige vragen geformuleerd teneinde het eindproduct vlot te kunnen integreren in het concrete project (bv. verwerking met GIS, ... zo is het bijvoorbeeld belangrijk om met (ascii-) data verdere berekeningen in een project te kunnen uitvoeren

2. **Omdat het welslagen van dit project afhangt van het uiteindelijke inzetten van het eindproduct in projecten van de eindgebruiker (IMDC), zal niet enkel het technische aspect belangrijk zijn, maar ook het financiële. Daarom wordt er voorgesteld om een business-case uit te werken waarin voor de verschillende gebruikscenario's (bv. gebaseerd op een vliegtuigvlucht, of op SPOT-beelden) de totale kostprijs van een set SSC-beelden wordt berekend (aankoop beelden, pre- en postprocessing).**

   De gevraagde business-case werd uitgewerkt (zie bijlage 7).

3. **In het kader daarvan zal het ook nodig blijken te zijn een afschatting te maken van hoeveel SSC-metingen (ground truth) er minimaal nodig zijn om de vereiste nauwkeurigheid te halen.**

   In bijlage 3 van het tussentijdsrapport werd getracht om op zowel statistische als op meer empirische wijze een antwoord te geven op deze vraag.

4. **Gezien het feit dat het hier om een onderzoeksproject gaat, is het ook belangrijk dat er in de eindraportage aandacht wordt besteed aan de pistes die het uiteindelijk niet gehaald hebben, en waarom. Denken we bijvoorbeeld aan de selectie van het gepaste algoritme om SSC aan reflectie-gegevens te koppelen. Voor latere referentie zal het zeker interessant zijn om aan te geven welke pistes geen of weinig resultaat hebben opgeleverd.**

   We zouden hier willen verwijzen naar paragraaf 1.3 van het tussentijdsrapport. Tevens wordt onder paragraaf 1.2.3.2 dieper ingegaan op de algoritmes die werden uitgetest.

5. **Hoewel het hier wel degelijk over de ontwikkeling van nieuwe technologie gaat, kan het waardevol blijken om contact te zoeken met de andere onderzoeksgroepen die met vergelijkbaar onderzoek bezig zijn:**

   - **BMM (Kevin Ruddick, BE)**
   - **NIOO (Herman Gons, NL)**
   - **Instituut van milieuvraagstukken (Hans van der Woerdt, NL)**

   Door onze betrokkenheid bij het BELCOLOUR project (http://www.mumm.ac.be/BELCOLOUR/) hebben we reeds regelmatig contact met BMM. In het kader van workshops georganiseerd omtrent het BELCOLOUR project hebben we ook al kennis gemaakt met NIOO en IVM. Met een voormalige werknemer van IVM (nl. Reinold Pasterkamp) hebben we tevens regelmatig via e-mail discussies gevoerd omtrent het opmeten van de specifieke inherente optische eigenschappen (SIOP). Het kan inderdaad echter interessant zijn om met hen een dieper in te gaan op de resultaten bekomen in het kader van het ORMES project.

6. **Een mogelijk zwak punt in de huidige aanpak is de validatie van de methode. Deze gebeurt momenteel met een "leave one out" techniek, wat eigenlijk betekent dat zowel calibratie als validatie met één enkele dataset gebeuren. Zeker in het licht van het feit dat de methode uiteindelijk breed inzetbaar moet zijn, is het belangrijk om de validatie zo breed mogelijk op te vatten. Een link naar de dataset van Qatar is een mogelijke optie, een geopperd alternatief was om gebruik te maken van de dataset van de "HCBS2" meetcampagne, die wordt georganiseerd door IMDC, iov het WLH in de week van 20 maart 2006.**

   Tot op heden beschikken we slechts over 1 grote dataset, waardoor de validatie inderdaad beperkt is. SPOT beelden van de Schelde (in het kader van de HCBS2 meet campagne) werden besteld maar onze aanvraag werd niet weerhouden door SPOTImage. Later werden nog pogingen ondernomen om SPOT en Formosat beelden van de Botlek haven te verkrijgen, maar ook deze keer werd het geen succes.
   Bijkomend aan de validatie met extra datasets, werd er reeds een gevoeligheidsanalyse uitgevoerd door monte carlo simulatie (ANNEX 4.1). Bovendien werd de meerwaarde van atmosferische correctie bestudeerd (ANNEX 4.3), tenslotte werd gebruik gemaakt van een gesimuleerde dataset om invloed van chlorofyl en 'adjacency' te onderzoeken.

7. **Naast de extra validatie is het ook waardevol om te zoeken of de algemene patronen die uit de SSC-beelden te voorschijn komen, worden gedekt door vroegere meetcampagnes op de Schelde. Zo kan er gekeken worden naar de**

gemeten dwarsgradienten van de oppervlakteconcentraties (linkeroever-rechteroever).

Het is inderdaad de bedoeling om extra validatie uit te voeren van de zwevende stofbeelden met behulp van transect informatie. De resultaten hiervan worden gegeven in bijlage 8.

ANNEX 2 – BACKGROUND ON REMOTE SENSING

Electromagnetic energy

In remote sensing, we classify electromagnetic energy by its wavelength. Visible light is the type of electromagnetic energy with which we are most familiar, but there is much to be learned from waves whose wavelengths are longer or shorter that those of visible light. In table 1 the names and wavelength region of electro-magnetic radiation are shown.

Electromagnetic energy interacts with the atmosphere and with the earth surface. All matter reflects, absorbs, penetrates and emits the electro-magnetic radiation in a unique way.

Table 1: Wavelength regions of electromagnetic radiation

class				wavelength	frequency
ultraviolet				100A ~ 0.4 μm	750 ~ 3,000 THz
visible				0.4 ~ 0.7 μm	430 ~ 750 THz
infrared	near infrared			0.7 ~ 1.3 μm	230 ~ 430 THz
	short wave infrared			1.3 ~ 3 μm	100 ~ 230 THz
	intermediate infrared			3 ~ 8 μm	38 ~ 100 THz
	thermal infrared			8 ~ 14 μm	22 ~ 38 THz
	far infrared			14 μm ~ 1 mm	0.3 ~ 22 THz
radio wave	submillimeter			0.1 ~ 1 mm	3 ~ 3 THz
	micro wave	millimeter	(EHF)	1 ~ 10 mm	30 ~ 300 GHz
		centimeter	(SHF)	1 ~ 10 cm	3 ~ 30 GHz
		decimeter	(UHF)	0.1 ~ 1 m	0.3 ~ 3 GHz
	very short wave		(VHF)	1 ~ 10 m	30 ~ 300 MHz
	short wave		(HF)	10 ~ 100 m	3 ~ 30 MHz
	medium wave		(MF)	0.1 ~ 1 km	0.3 ~ 3 MHz
	long wave		(LF)	1 ~ 10 km	30 ~ 300 KHz
	very long wave		(VLF)	10 ~ 100 km	3 ~ 30 KHz

Reflectance

Reflectance is then defined as the ratio of incident flux on a sample surface to reflected flux from the surface as shown in Fig.1. Reflectance ranges from 0 to 1.

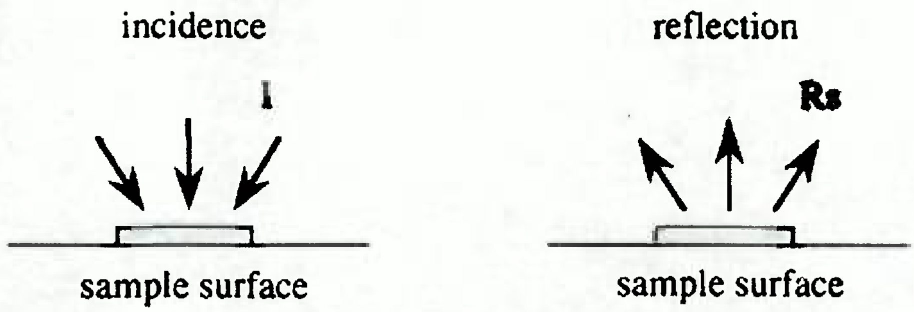

reflectance = Rs /I

Figure 11: Definition of reflectance

Reflectance with respect to wavelength is called spectral reflectance (or spectrum) as shown for a vegetation example in Fig.2.

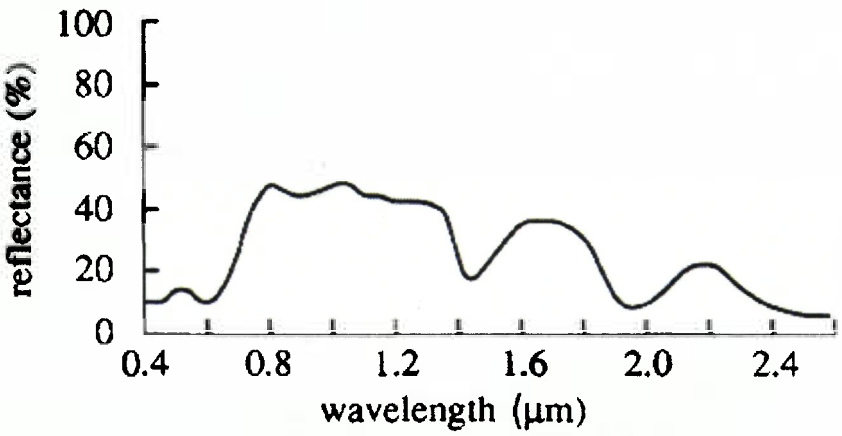

Figure 2: Vegetation spectrum

Spectral reflectance is assumed to be different with respect to the type of land cover. This is the principle that in many cases allows the identification of land covers with remote sensing by observing the spectral reflectance or spectral radiance from a distance far removed from the surface.(El Laboratorio de Procesos Oceanográficos y Clima (PROFC), 2006)

http://www.profc.udec.cl/~gabriel/tutoriales/rsnote/contents.htm

Hyperspectral remote sensing

A spectral band is a well-defined, continuous wavelength range in the spectrum of reflected or radiated electromagnetic energy. Multispectral sensors sample the EM spectrum over a relatively wide range of wavelengths in discrete bands. These sensors therefore have low spectral resolution. Hyperspectral sensors sample the electromagnetic spectrum in many narrow bands. Hence, for each picture element in a hyperspectral image it is possible to derive a complete reflectance spectrum (Goetz, 1992). Each picture element contains a unique reflectance spectrum which can be used for the identification of Earth's surface materials. The principle of hyperspectral remote sensing is shown in Fig.3. (Hyperteach, 2005)

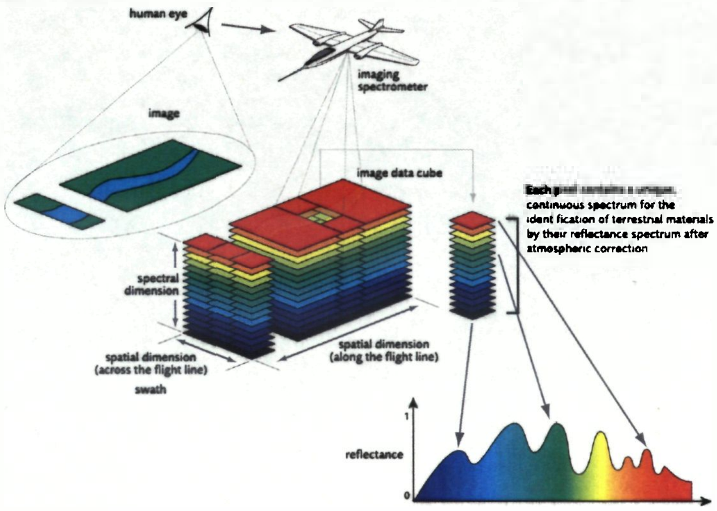

Figure 3: principle of hyperspectral remote sensing

ANNEX 3 - DETERMINATION OF MINIMUM SAMPLE SIZE.

The question we would like to be answered is "How many samples should be considered to estimate the TSM concentrations with a pre-defined accuracy?" It is of course important to determine the adequate sample size, because without these calculations sample size will be too high are too low. If sample size is too low, no conclusions can be made on the significance of the relationship. In general, increasing sample size means increasing costs, both in time, money, and effort. Consequently, it is important to make sample size "large enough," but not wastefully large.

First, we would like to answer this question on a statistical basis. Secondly we use our dataset of water samples to find this sample size in a more empirical way.

Statistical test

To answer this question for our specific study case a literature review was performed. However no exact answer to our question could be found. All related literature comes from the behavioral sciences where it is tested how many samples are needed (1) to know that the correlation coefficient is not zero (this means there is a correlation) or (2) that the correlation coefficient falls within a pre-defined range.

For case (1), several rules of thumb have been presented (Green, 1991):

$N <= 50 + 8m$ [1]

$N >= L/f^2$ with $L = 6.4 + 1.65m - 0.05m^2$ and $f^2 = R^2/(1-R^2)$ [2]

with m the number of predictors.

In our case with only one predictor 'the reflectance index' and and $R^2=0.83$, the minimum number of samples should be 58 according to formula (1) and 2.2 according to formula (2).

To calculate the necessary sample size such that the confidence interval of the population correlation coefficient is sufficient precise, sample size tables reported in Algina and Olejnik (2003) can be consulted (table 1):

Table 1 Sample size necessary for the correlation coefficient to falls within a pre-defined range

Table 1
Sample Sizes Necessary to Meet Target Accuracy for: ρ = .95: Distribution of r

	c			
ρ	.05	.10	.15	.20
0.00	1538	385	172	97
0.05	1530	383	171	97
0.10	1507	378	168	95
0.15	1469	368	164	93
0.20	1417	355	159	90
0.25	1352	339	151	86
0.30	1274	319	143	81
0.35	1185	[illegible]	133	75
0.40	1086	273	122	69
0.45	979	246	110	63
0.50	866	218	98	56
0.55	750	189	85	49
0.60	632	160	72	42
0.65	515	131	60	35
0.70	402	103	47	28
0.75	297	77	36	23
0.80	202	[illegible]	27	18
0.85	120	34	19	13
0.90	60	20	12	9
0.95	21	9	6	5

For our case (correlation coefficient (ρ) of 0.91, confidence limits (c) of 0.05) the sample size (n) is +/- = **60**. The sample size decreases strongly when the total width of the confidence interval (c) increases.

Still, a good estimate of R^2 doesn't imply a good estimate of TSM concentrations.

TSM concentrations are better estimated

1. when R^2 is larger because the total variation of Y is reduced more by introducing the predictor variable X
2. When regression coefficients are well estimated.

For estimating the regression coefficients, the spacing of the independent variables has to be taken into account. In our case, it is clear that the regression analysis can give strongly biased results when only spectra are included which are taken at places with either very high or very low concentrations. To avoid such biased results Neter *et al.* (1996) suggest to include sample points at the two extremes and the other sample points should be well divided round mean.

Empirical test

A **leaf-N-out** procedure was used to test how the errors in the SPM estimates for new observations (= not used in the regression analysis) were effected when the number of samples used in the construction of the regression equation decreased from 41 down till only 2 samples.

Out of the set of 41 SPM values (derived from water samples) and corresponding image reflectance spectra smaller subsets were selected ranging from 2 to 25 samples (k). The number of possible subsets of k samples from a set of 41 can be calculated as 41!/(k!*(41-k!)). As long as the number of possible subsets was below 100million, all possible subsets were subsequently used. When the number of possible subsets was above this number, 500000 subsets were randomly selected as computer memory limits don't allow the use of all possible combinations.

For each subset the difference term (R(0-,833) - R(0-,1004)) was regressed against ln(SPM) and the regression equation was determined. With this regression relationship the SPM concentration was estimated for the *remaining* dataset and compared to the measured SPM concentrations in order to retrieve the errors (RMSE[2]) on the estimated values. As these RMSEs were calculated for a very large number of subsets of a specific sample size, histograms of the RMSEs can be constructed for each sample size. In figure 1 histograms of the errors are constructed for respectively a sample size of 3, 4, 5 and 6. Each histogram shows a peak frequency at a RMSE of +/- 14 mg/l.

[2] In this section RMSE is the RMSE of the samples not used in the regression equation determination

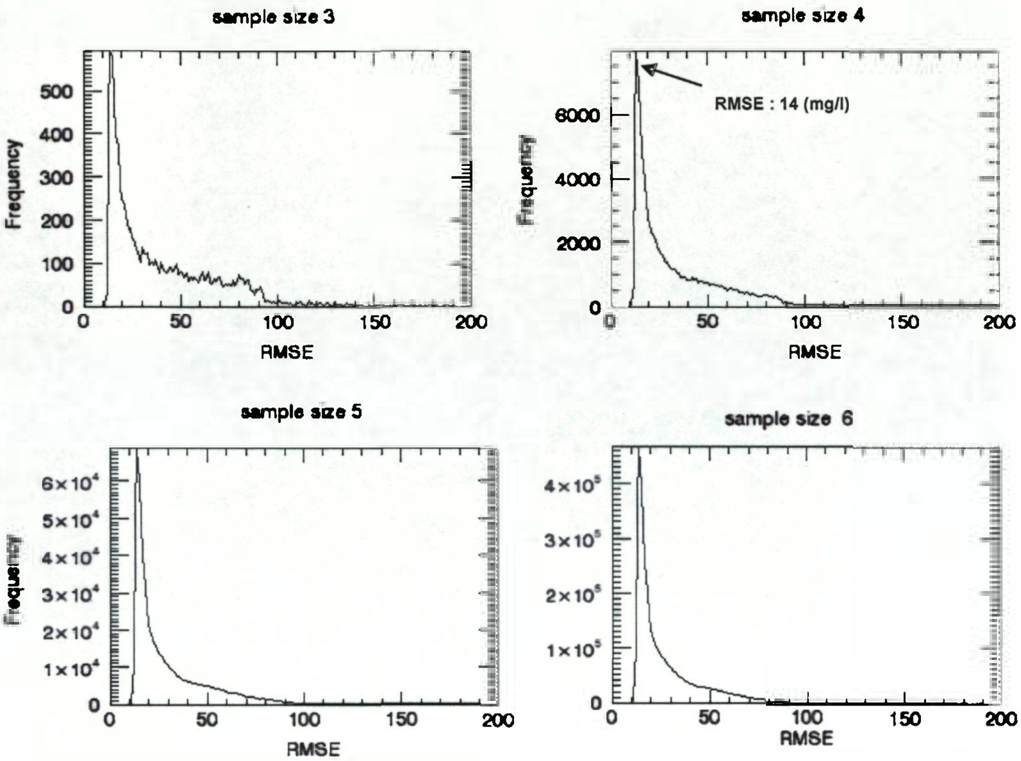

Figure 1: Histograms of RMSE (of the remaining dataset) for different sample sizes.

One subset of 4 samples resulting in a RMSE of approximately 14 mg/l for the remaining samples was randomly selected and the coefficients of the regression of the difference term (R(0-,833) - R(0-,1004)) against ln(SPM) were determined. This gives the following regression equation :

$$\mathrm{Ln(SPM)} = 39.85*(R(0-,833)-R(0-,1004)) + 3.32 \qquad [3]$$

The original equation which was determined using all 41 samples was :

$$\mathrm{Ln(SPM)} = 34.18*(R(0-,833)-R(0-,1004)) + 3.16 \qquad [4]$$

Both algorithms were applied to an image to illustrate the effect on the resulting SPM maps (Figure 2). Overall distribution of SPM is comparable however the SPM map created with algorithm [3] shows higher concentrations. The histogram of the difference image (calculated as |(SPM_algorithm3 – SPM_algorithm4) * 100/SPM_algorithm3|) indicates that most differences are in the range of 30 -40% (Figure 3).

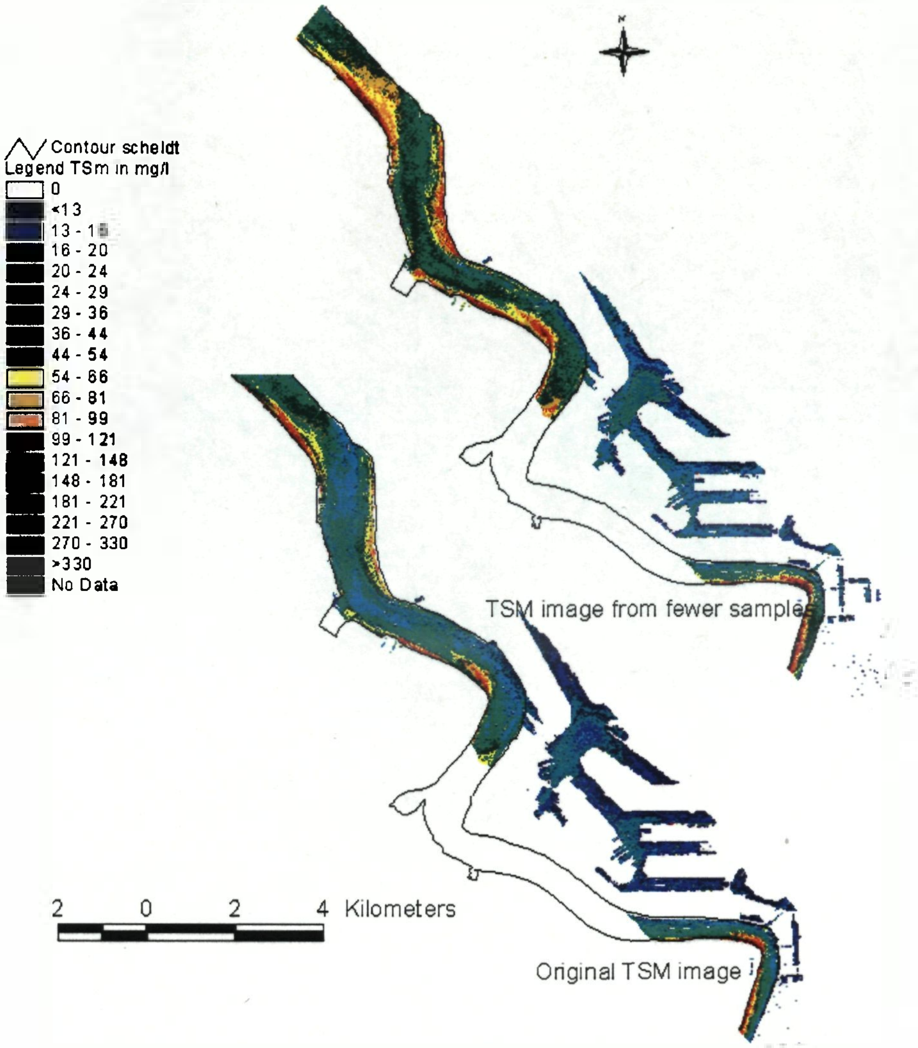

Figure 2: SPM maps created with the original algorithm (algorithm 3) and with an algorithm based on only 4 samples (algorithm 4).

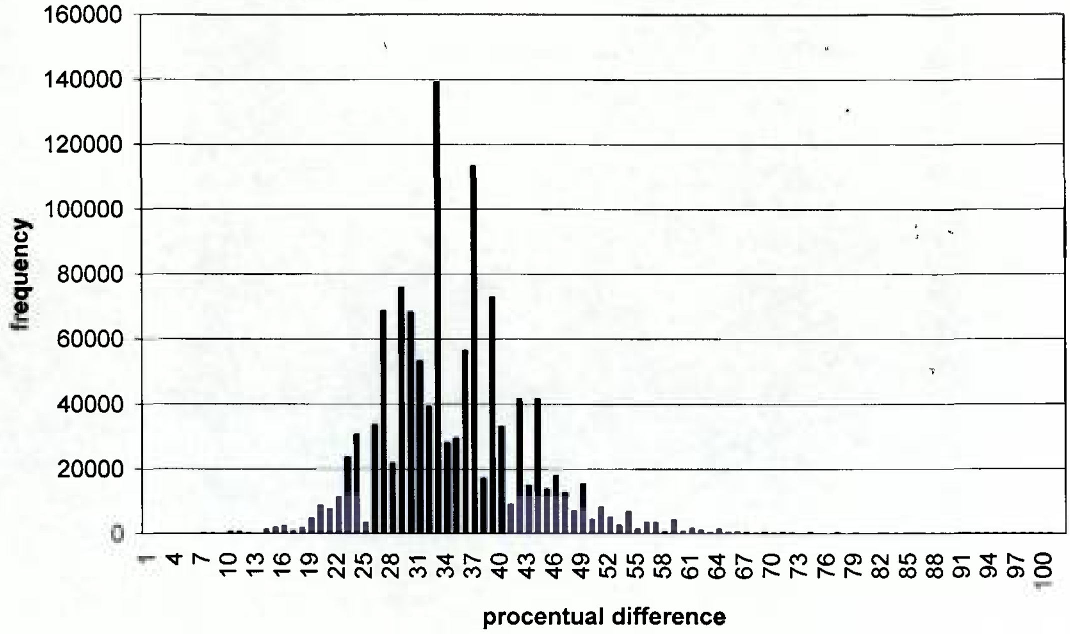

Figure 3: Histogram of the difference image of |(SPM_algorithm3 – SPM_algorithm4) * 100/SPM_algorithm3|.

In table 2 and figure 4 the percentage of subsets resulting in a RMSE (for the remaining dataset) of maximum 20 and 30 mg/l are given. If 8 samples are randomly selected there is more than 80 % chance that the regression equation (ie. (R(0-,833) - R(0-,1004)) vs ln(SPM) based on these 8 samples can predict the SPM for the remaining dataset with a RMSE of less than 30 mg/l. As the number of samples in the dataset increases, the chance of predicting the remaining SPM values with a RMSE of less than 20 or 30 mg/l percentages increases asymptotically. The graph indicates that for sample sizes lower than 8 the chance of predicting the remaining SPM values with a RMSE of less than 20 or 30 mg/l increases strongly by adding an extra sample. For larger datasets the adding of an extra sample only slightly increases the RMSE. However this does not mean that a regression based on a sample size of only 4 can not give good estimation. If only a few samples can be taken it is of high importance to cover the suspended range within the area as good as possible. Figure 5 shows a situation where 4 well-distributed samples are enough to predict the SPM for the remaining dataset with a RMSE of only 11 mg/l.

(?) A priori knowledge of SPM of samples

Is het mogelijk om de sites a [illegible] te kiezen dat de hele SPM range is gecovered?

Zonder die a priori kennis is de kans om met 4 samples een RMSE v. 11 te halen [illegible] !

Table 2 : Percentage of all subsets resulting in a RMSE (for the remaining dataset) of maximum 20 and 30 mg/l are given

Sample size	Percentage of subsets with RMSE ≤ 20 mg/l	Percentage of subsets with RMSE ≤ 30 mg/l
2	21.61 %	32.47 %
3	32.08 %	47.18 %
4	41.04 %	58.35 %
5	47.87 %	66.37 %
6	53.26 %	72.27 %
7	57.58 %	76.74 %
8	61.22 %	80.27 %
9	64.11 %	83.09 %
10	66.31 %	85.03 %
11	68.36 %	86.78 %
12	69.97 %	88.26 %
13	71.31 %	89.48 %
14	72.43 %	90.36 %
15	73.49 %	91.21 %
16	74.29 %	91.92 %
17	74.86 %	92.45 %
18	75.51 %	93.00 %
19	75.92 %	93.40 %
20	76.31 %	93.75 %
21	76.40 %	94.05 %
22	76.73 %	94.37 %
23	76.71 %	94.58 %
24	76.73 %	94.79 %
25	76.6 %	94.87 %

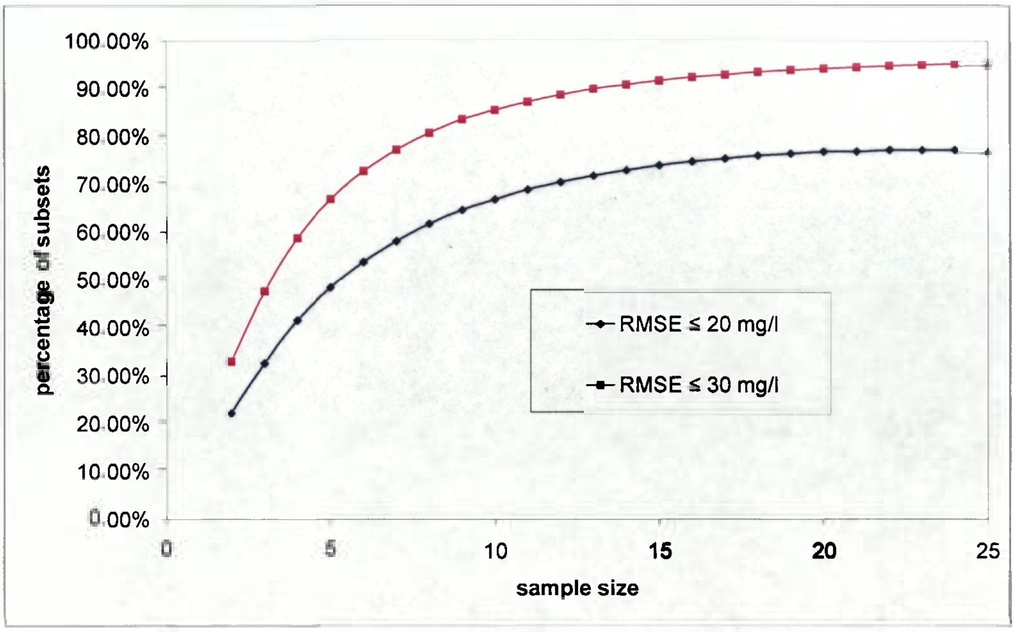

Figure 4: Graphical representation of percentage of all subsets resulting in a RMSE (for the remaining dataset) of maximum 20 and 30 mg/l are given

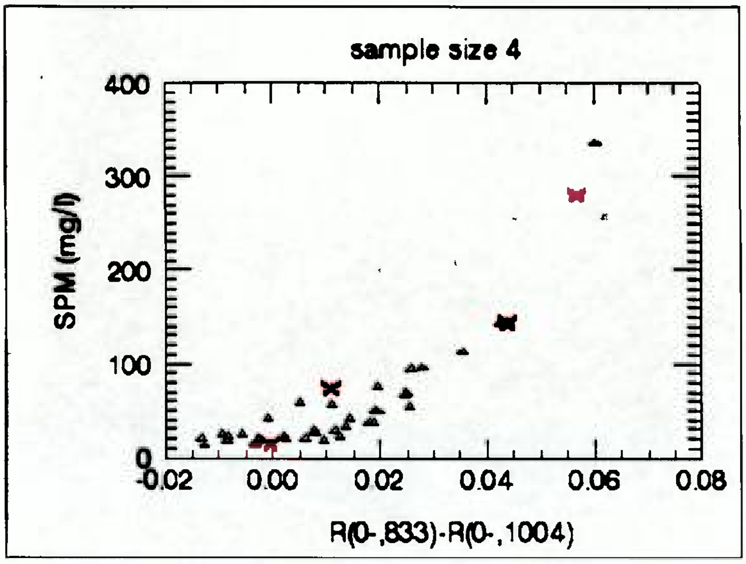

Figure 5: The location of 4 well-distributed samples which result in a RMSE of 11 mg/l for the remaining dataset.

References

Algina, J. and S. Olejnik, 2003, Sample size tables for correlation analysis with applications in partial correlation and multiple regression analysis, Multivariate Behavioral research, 38(3), 309-323.

Green, S., 1991, how many subjects does it take to do a regression analysis? Multivariate Behavioral research, 26(3), 499-510.

Kelley, K. & Maxwell, S.E. (2003). Sample size for multiple regression: Obtaining regression coefficients that are accurate, not simply significant. *Psychological Methods*, *8*, 305--321.

Neter, J. et al.,1996. Applied Linear statistical models, fourth edition

http://www.stat.ucla.edu/

ANNEX 4 - SENSITIVITY ANALYSIS

1. Sensitivity analysis using Monte Carlo simulation

As described in section 1.2.3.2 the best fit between the image reflectance spectra and the SPM concentration determined from water samples was found to be a log-linear line fit to a band-difference i.e. ln(SPM) ~ R(0-,833)-R(0-,1004) with a correlation coefficient (R^2) of 0.83 and a root mean square error (RMSE) of 15.53 mg/l. A sensitivity analysis is performed to test: the robustness of this relationship to uncertainties in the inputs, or more precisely, how RMSE, R^2 and the final SPM maps respond to these uncertainties. The inputs are, in our case, the set of 41 reflectance spectra and SPM concentrations derived from water samples. In this research, the sensitivity analysis is done with Monte Carlo simulations which generates uncertainty values for the inputs over and over.

A. Effect of errors in input SPM and reflectance spectra on R^2 and RMSE

Errors were added to the SPM concentrations and/or reflectances. These errors were

1) randomly selected from a normal distribution (10%, 10%+, 20% random)

and/or

2) systematic (10%, 20% biased)

In each random case (e.g. 10 % random error SPM), 10000 different sets of inputs (SPM versus reflectances) were created and each input set was subsequently used in the regression analysis. For each set, the natural logarithm of the SPM concentrations was linearly regressed against [R(833) – R(1004)] (cfr. Algorithm [1]) and the RMSE and R^2 values were determined. Finally, a histogram was constructed for the 10000 R^2 and RMSE values of the regression analysis (Figures 1-6). In table 1 standard deviation and mean value of the R^2 and RMSE are summarized for each case. When 10% random error is incorporated in SPM, in reflectance or in both, changes in R^2 and RMSE are relatively small. Only when 20% random error is added to the reflectances the mean RMSE increases significantly. Overall, RMSE seems to be more sensitive to errors in reflectance values than to errors in SPM.

Table 1: Mean and standard deviation

Error	correlation coefficient mean	stdev	RMSE mean	stdev
SPM				
10% random	0.82	0.01	17.55	2.36
20% random	0.78	0.03	22.64	4.82
10% bias	0.83	0.00	17.09	
20% bias	0.83	0.00	18.65	
10% random +	0.83	0.01	17.44	1.58
reflectance				
10% random	0.82	0.01	20.37	4.70
20%random	0.79	0.03	28.28	8.75
reflectance and SPM				
10% random	0.82	0.01	16.92	1.99
20%random	0.80	0.03	20.93	5.50

Note 10% random error is normally distributed with a mean error of 0 % and a standard deviation of 10 %; 10 % bias: fixed error of 10%

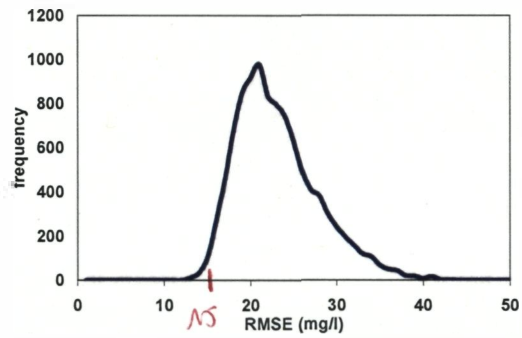

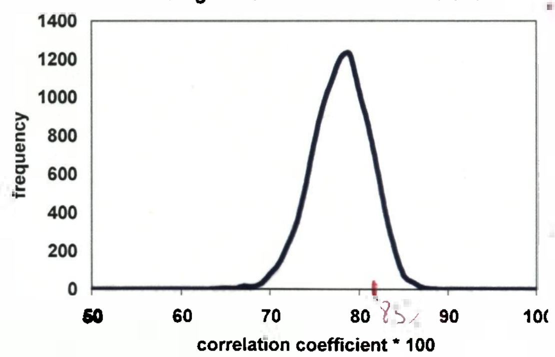

Figure 1: Random 20 % error introduced in SPM concentrations, 10000 runs

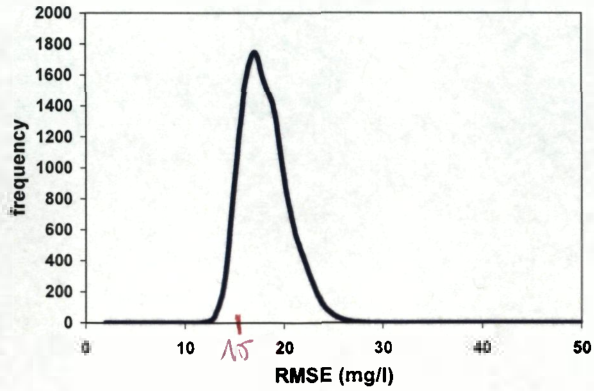

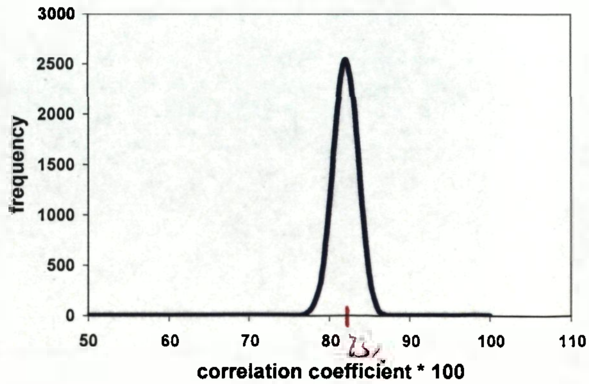

Figure 2: Random 10 % error introduced in SPM concentrations, 10000 runs

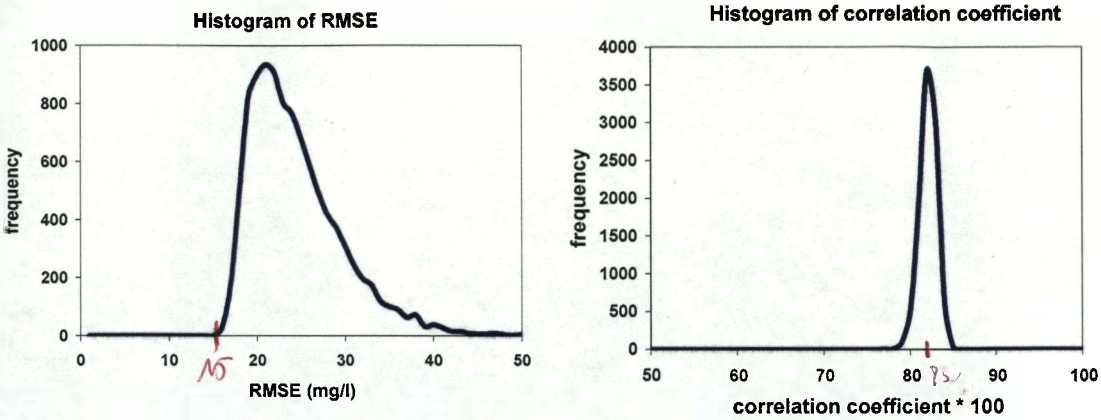

Figure 3: Random 10% error introduced in reflectance, 10000 runs

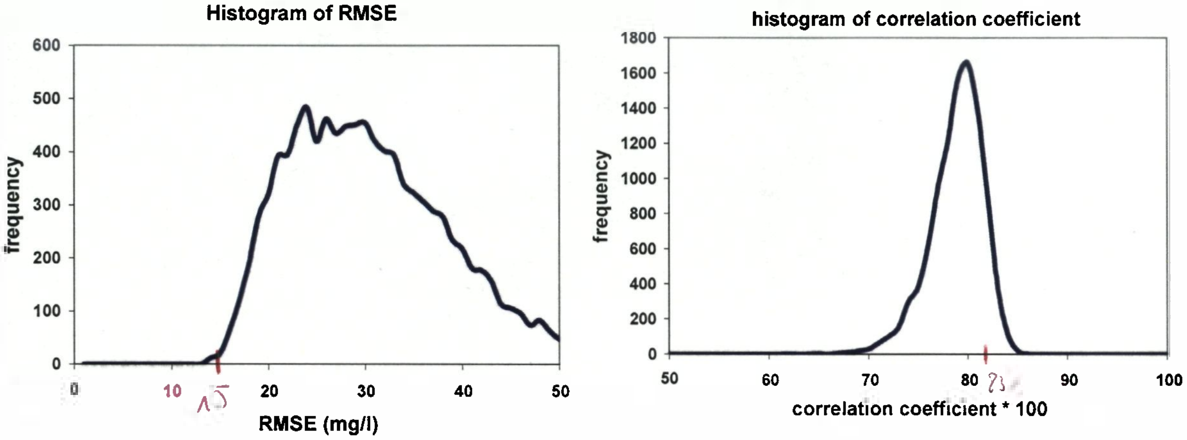

Figure 4: Random 20% error introduced in reflectance, 10000 runs

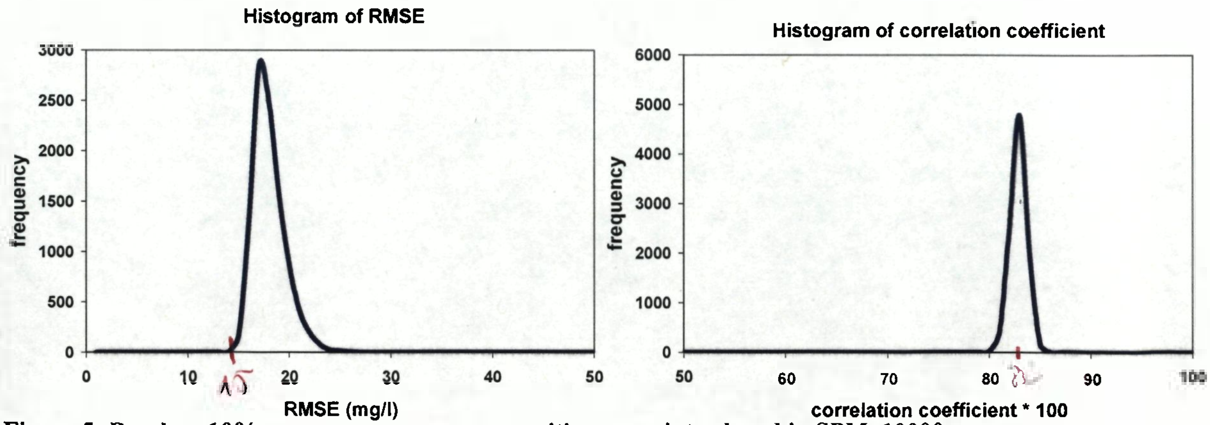

Figure 5: Random 10% positive error introduced in SPM, 10000 runs

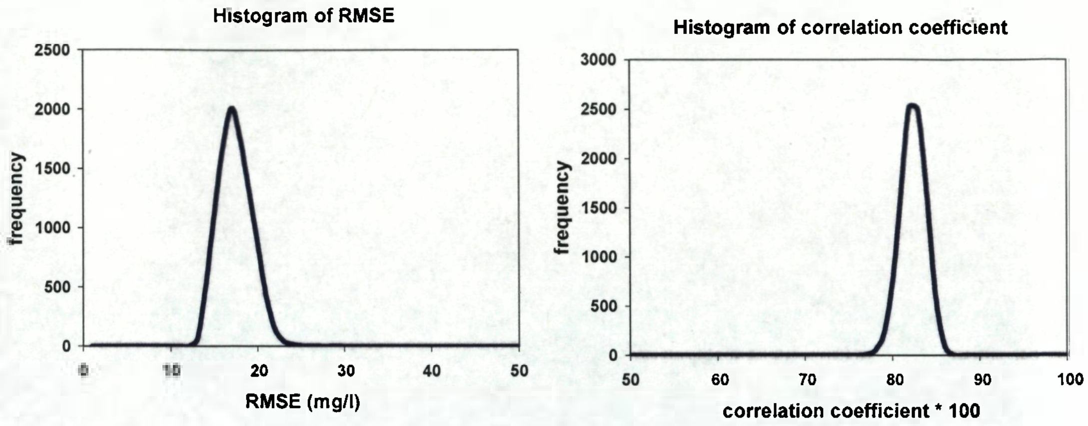

Figure 6: Random 10% error introduced in reflectance and SPM, 10000 runs

B. Effect on final SPM map

To visually illustrate the effect of 20% random error in the input SPM on the final TSM maps the regression coefficients were selected for the case where:

$R^2 = \mu - 2 * s$ **and** $RMSE = \mu + 2 * s$

with μ mean and s standard deviation.

The algorithm becomes:

$$Ln(SPM) = 3.12 + 39.23 * (R(833) - R(1004)) \qquad [1]$$

This algorithm is applied to images taken at 2 different moments in the tidal cycle i.e. 08:21 UTC and 10:03 UTC. The resulting SPM maps are then compared to the original SPM maps (i.e. without uncertainties in input parameters) by creating a SPM difference image (Figure 7 and 8) with the difference calculated as :

|(original SPM-new SPM)*100/original SPM|.

The distribution of these difference values are also given in histogram format (figure 8 and 10).

Effects of incorporating a quite large error (s = 20%) in the inputs are rather small. Single values can differ up to 30% in turbid areas but most errors are in the range of 0-15 % . The overall patterns are still clearly recognizable.

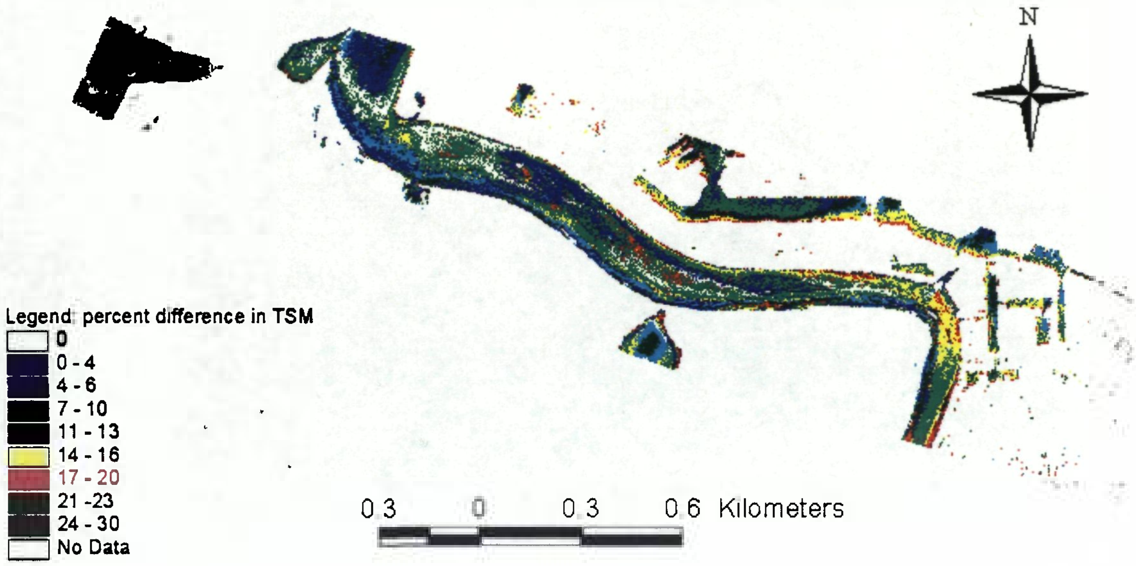

Figure 7: Difference image at 08:21 UTC

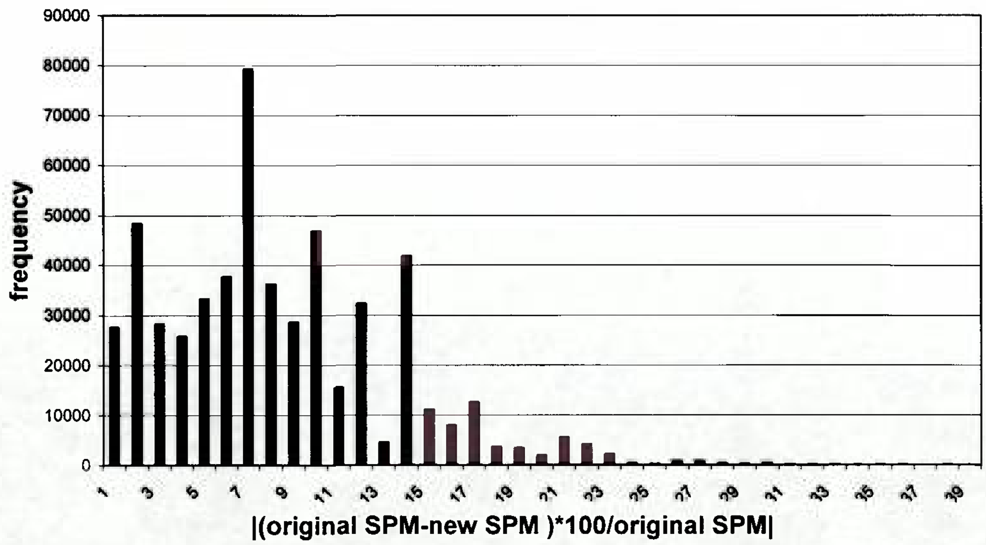

Figure 8: Histogram of Difference image at 08:21 UTC

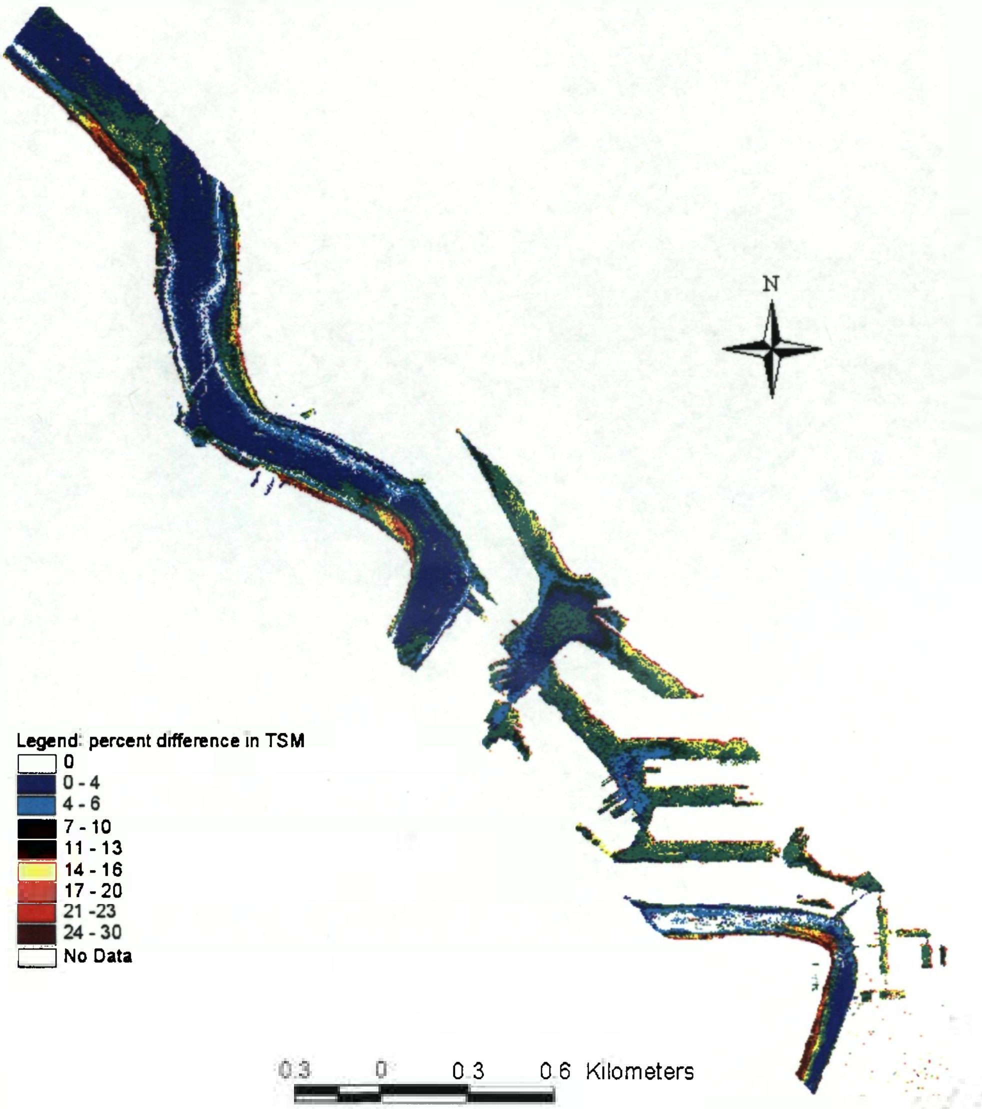

Figure 9: Difference image at 10:03UTC

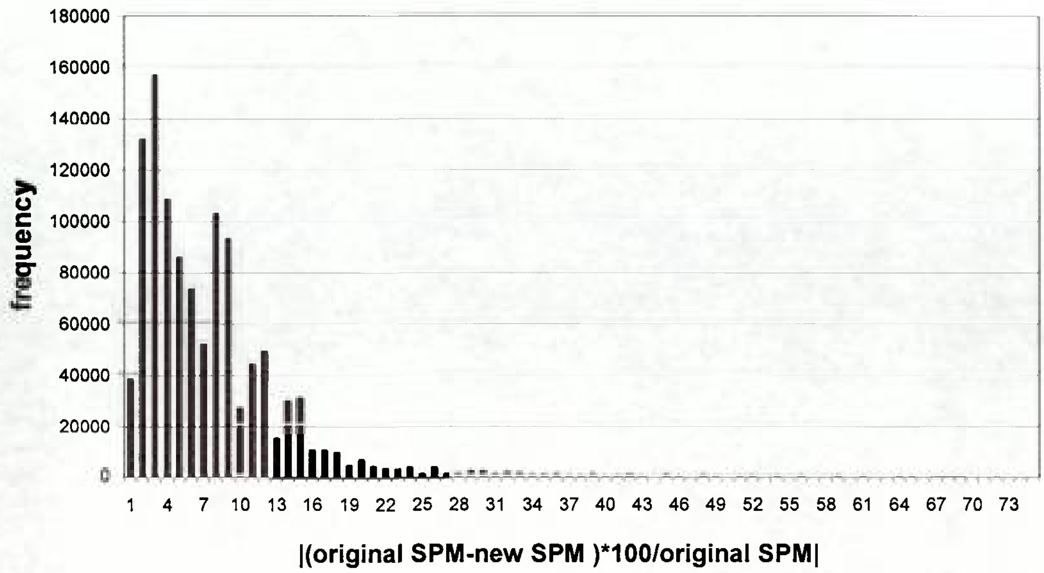

Figure 10: Histogram of difference image at 10:03 UTC

2. Influence of the atmosphere

To perform atmospheric and air-interface corrections specific software is required. Hence, it is interesting to know if we still can get satisfying results without these corrections and thus minimizing the processing time and associated cost.

At-sensor radiance spectra (L) were extracted from the uncorrected images - without atmospheric and air/interface correction- at the sampling locations and regression analysis were performed using the SPM concentrations determined from the water samples.

The band difference SPM algorithm i.e. ln(SPM) ~ R(0-,833)-R(0-,1004) that performed best for the atmospherically corrected images gave for the uncorrected dataset a R^2 of only 0.72, a RMSE of 19.13 mg/l and a LOO-RMSE of 20.54 (35%) (Figure 11):

Ln(SPM)= (L(833)-L(1004)) *0.367 + 2.0351 **[2]**

Although some algorithms gave higher R^2 (up till 0.82), the RMSE was mostly quite high (between 20 and 30 mg/l), except for the following algorithm (Figure 12):

Ln (SPM) = (L(833)/L(1004)) *3.03 -1.70 [3]

with R^2 = 0.81, RMSE = 17.86, LOO-RMSE = 21.77 (34%) and where L(833) and L(1004) at sensor-radiance at 833 and 1004 respectively.

An interesting finding is that the best algorithm [3] derived for the uncorrected images makes use of the same spectral bands i.e. 833 and 1004 as the original algorithm derived for corrected images, but instead of a band difference a band ratio gave slightly better results

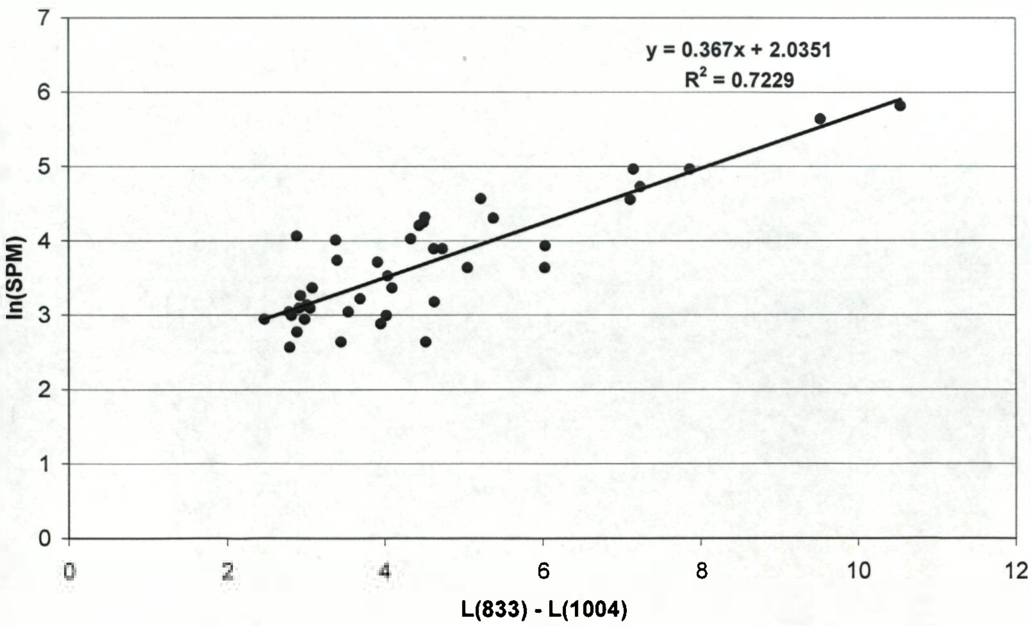

Figure 11: coefficients and R^2 for ln(SPM) ~ [L(0-,833)-L(0-,1004)]

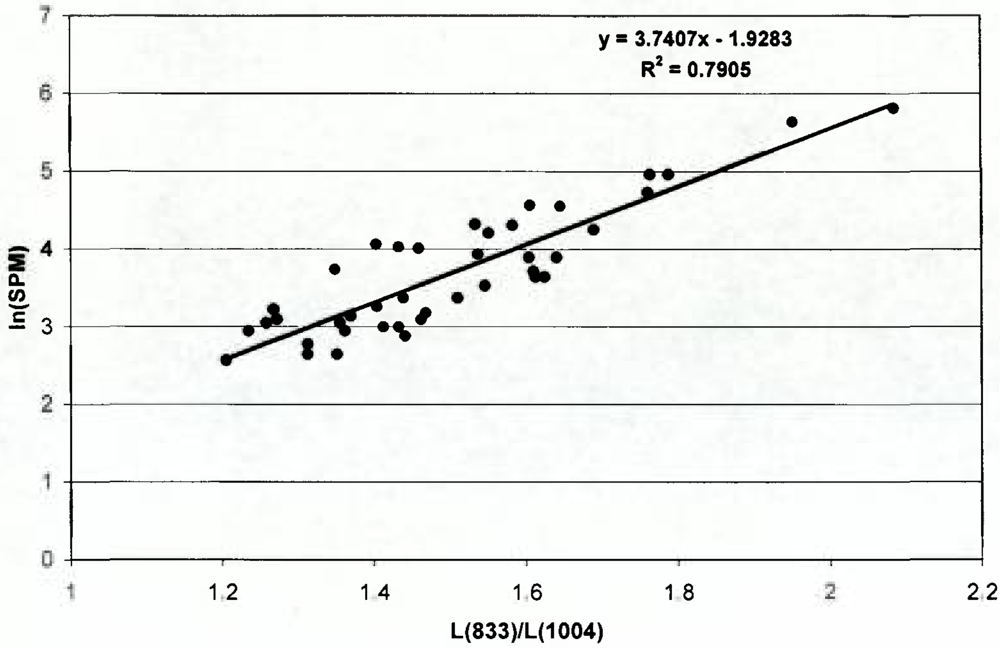

Figure 12: coefficients and R^2 for ln(SPM) ~ [L(0-,833) / L(0-,1004)]

In figure 13 comparison is given of the band ratio algorithm [3] (Fig.13a) and band difference algorithm [2] (Fig. 13c) applied to atmospherically uncorrected data and the original band difference algorithm applied to corrected data (Fig. 13b).

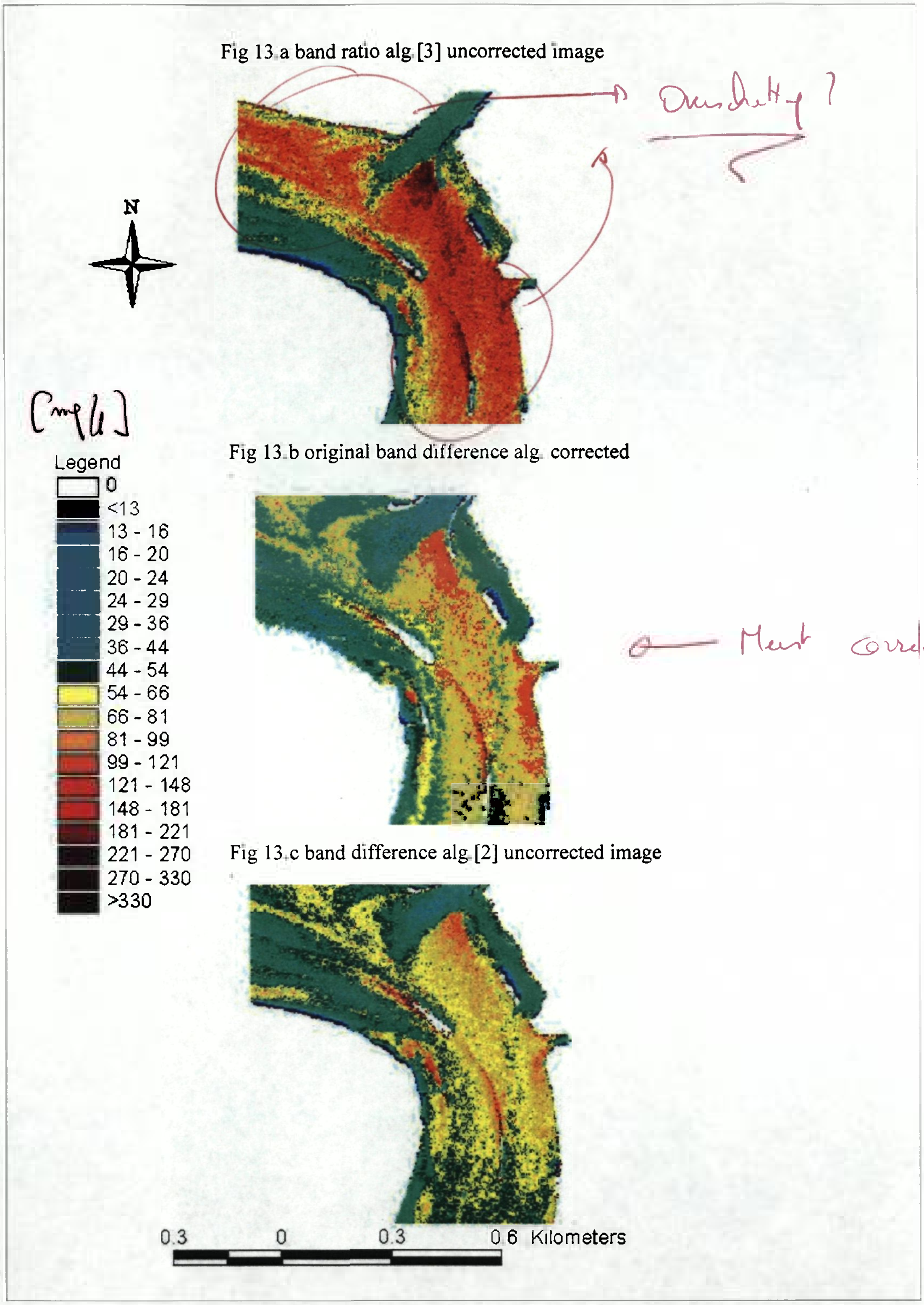

Figure 13: Comparison of SPM maps obtained with corrected and uncorrected datasets.

3. Simulated spectra

At-sensor radiance spectra, corresponding to large range of SPM and CHL concentrations, were simulated in order to test influence of chlorophyll variation and adjacency effects on the performance of the SPM algorithms. For the calculation of the at-sensor radiance spectra the following procedure was followed:

1. a set of about1000 [**SPM**, CHL] **concentrations**, ranging respectively between 0 and 300 mg/l and between 0 and 8 μg/l, was randomly created
2. this set of [SPM, CHL] concentrations were used as input to the reflectance model given by Albert and Mobley (2003) in order to generate **reflectance spectra** for different SPM and CHL concentrations.
3. with the radiative transfer code Modtran-4 atmospheric scattering and absorption was simulated in order to calculate **at-sensor radiance spectra (L)**. No atmospheric variability between the spectra was assumed i.e. atmospheric parameters remain constant.

   In order to study **adjacency effects** (i.e. the contribution of adjacent surfaces to the at-sensor radiance spectrum of the water pixel) two test sets were created :

   Test set 1 : background spectrum = water spectrum => +/- no adjacency

   Test set 2 : background spectrum = water, asphalt or dead grass spectrum (for each of the simulation one background type was randomly selected) => random variability of adjacency effect : no (water) – medium (asphalt) – high (grass)
4. Finally, the at-sensor radiance spectra (test set 1 and test set 2) were **resampled to the AHS** wavelengths

Single bands, band ratios, differences of 2 bands of the 3 test sets were linearly or logarithmically regressed against the input SPM concentrations and the R^2 and RMSE of these regression functions were noted. The best performing algorithms (judged on the basis of R^2 and RMSE) are summarized in table 2.

Table 2: Best performing algorithm for test set 1 and test set 2

Test set	Algorithm	R^2	RMSE
1: no adjacency	Single band algorithms : L(948) ~ SPM	0.999	1.36
2 : adjacency	Band difference algorithms : [L(833) - L(1004)] ~ SPM	0.99	8.36

For test set 1 (no adjacency) algorithms based on one single band perform very good. When adjacency effects are taken into account (test set 2) the performance of single band algorithms decrease strongly.

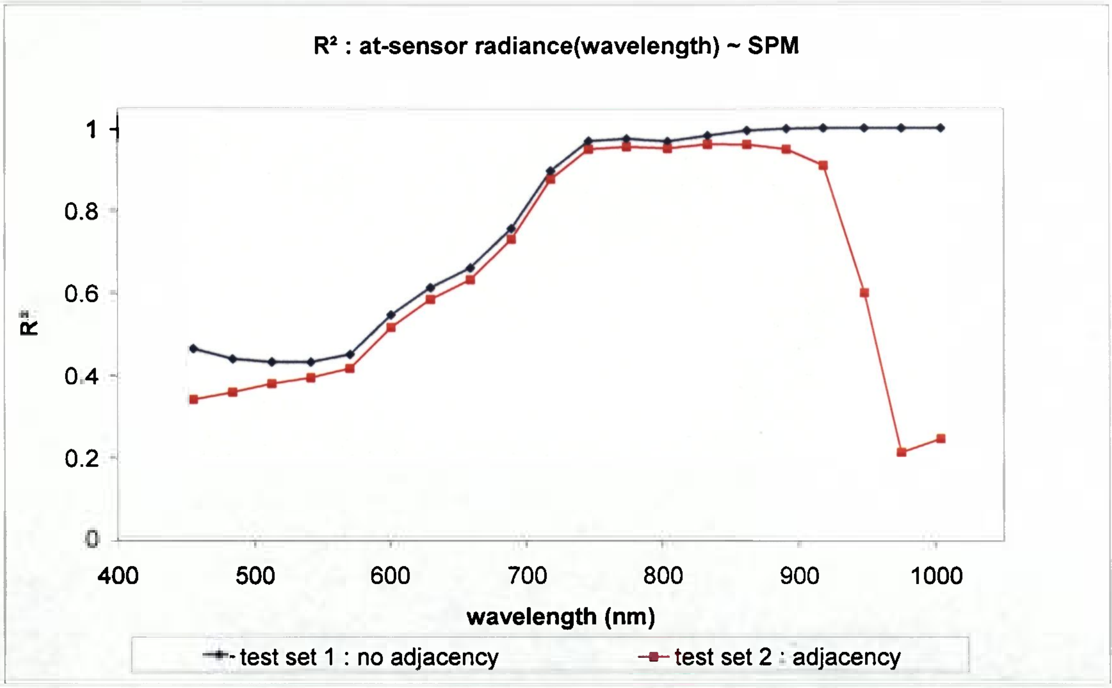

Figure 14: R^2 for single band radiance linearly regressed against SPM

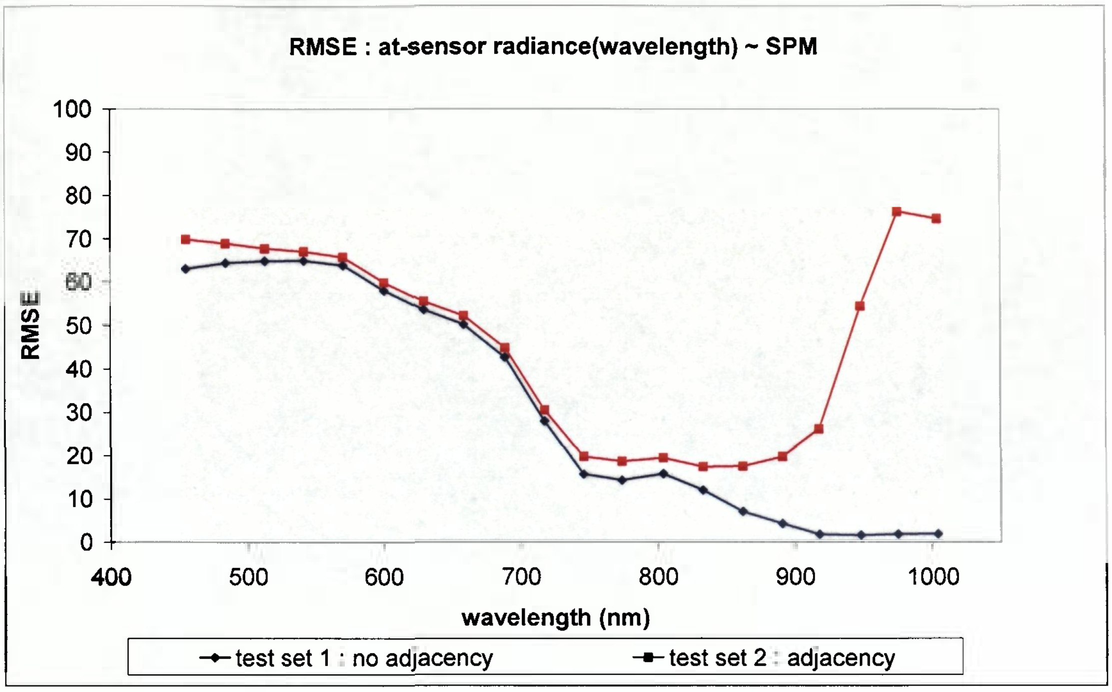

Figure 15 : R^2 for single band radiance linearly regressed against SPM

The R^2 and RMSE for the linear regression of single bands against SPM are respectively plotted in figure 14 and 15. These figures show that for *test set 1* all bands from 918 nm till 1004 nm gives R^2 of almost 1 and low RMSE. The inclusion of adjacency effects (*test set 2*) strongly decreases the R^2 for wavelengths larger than 900 nm and increases the RMSE. However with the use of **band difference algorithms** the influence of adjacency effects are minimized (table 2). Note that for for both the simulated and real dataset is the same bands are used in the best performing algorithm i.e. 833 and 1004.

The R^2 and RMSE of the SPM algorithms for the *simulated* AHS at-sensor radiance datasets are much better than for the *real* AHS at-sensor dataset (results in previous chapter). This is because the simulated spectra were not influenced by (1) sensor noise, (2) differences in atmospheric conditions (⇔ real data set strongly variable atmospheric conditions), (3) variation in optical properties of the sediment particles due to differences in the composition and grain size and (4) measurements uncertainties of the SPM concentration.

ANNEX 5 - WEATHER CONDITIONS AT THE DAY OF THE FLIGHT CAMPAIGN

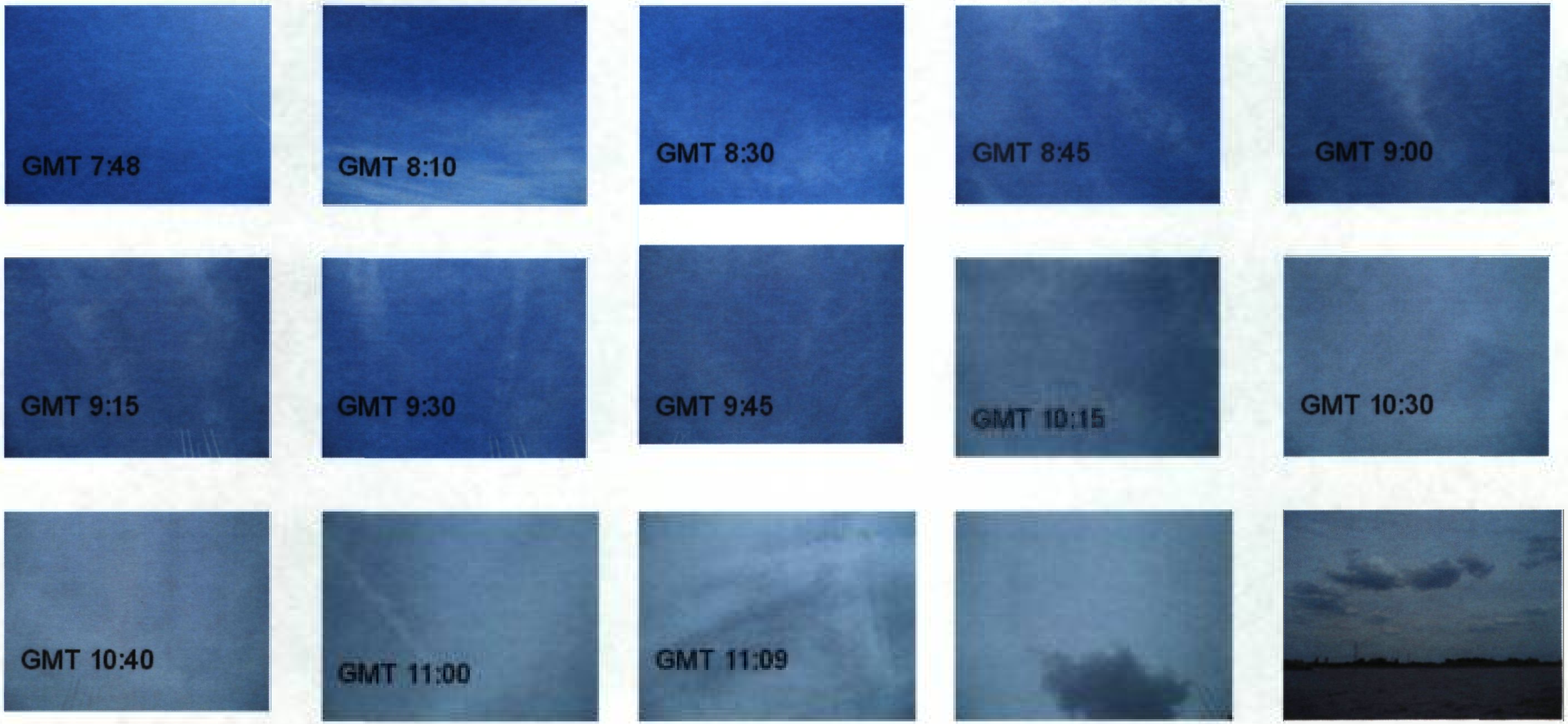

ANNEX 6 - AHS RESAMPLED TO SPOT AND LANDSAT

The hyperspectral AHS image was resampled spatially and spectrally to a SPOT5 HRV image and a Landsat TM7 image. The simulated SPOT image has a spatial resolution of 20m and 4 broad spectral bands (at 542nm, 654nm, 835nm and 1629 nm), the simulated Landsat image has a spatial resolution of 30m and 6 broad spectral bands (at 479nm, 561 nm, 661nm, 835 nm, 1651nm and 2209nm) (Figure 1).

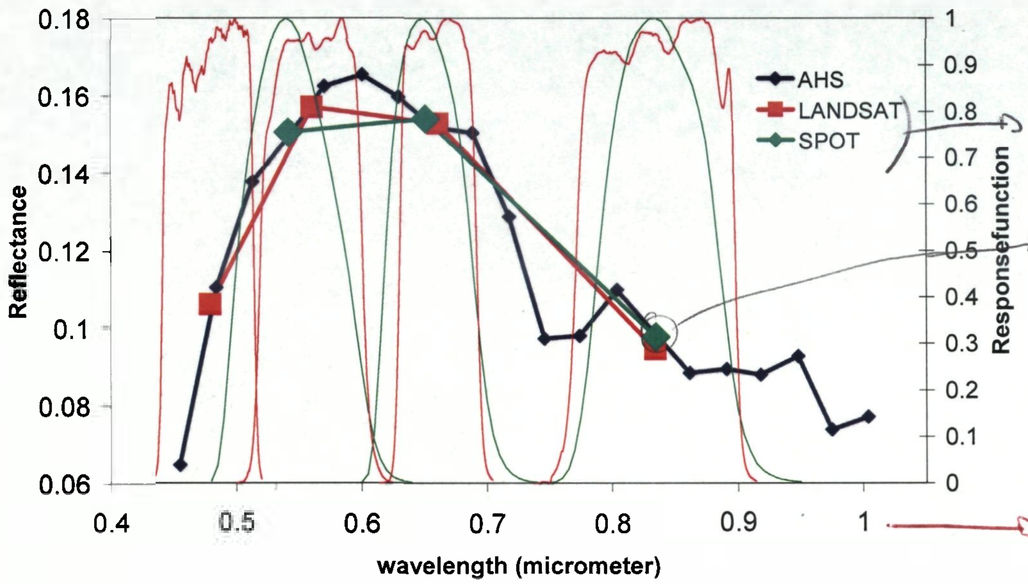

Figure 1: Spectral bands and response function of SPOT and Landsat uptill 1 μm

Again, correlations were calculated between different bands (or band combinations) and TSM. The following algorithm was selected to derive a TSM map for the SPOT image:

TSM (mg/l) = exp(-7.41 + 11.06 *(R(0-,652)/R(0-, 542)))

with a rmse of 32.40 mg/l and a determination coefficient (R^2) of 0.79. A similar algorithm was found for the Landsat image:

TSM (mg/l) = exp(-6.37 + 10.86 *(R(0-,661)/R(0-,561)))

With a RMSE of 29.05, a coefficient of determination (R^2) of 0.81.

For the image taken at 10:03 UTC, the results agree quite well with the SPM maps from the AHS but SPM concentrations are a little more extreme (Figure 3). For the image taken at 08:21 UTC TSM concentrations increase when resampled to SPOT and Landsat (Figure 2).

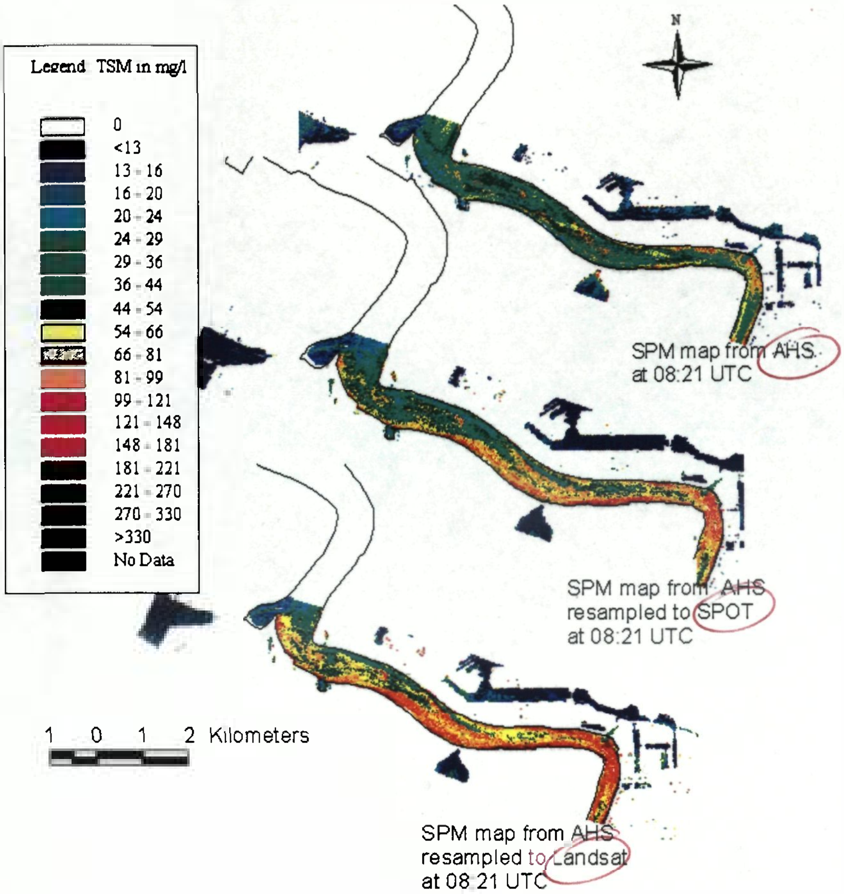

Figure 2 : Comparison of SPM maps derived from AHS data and AHS data spectrally and spatially resampled to SPOT and Landsat

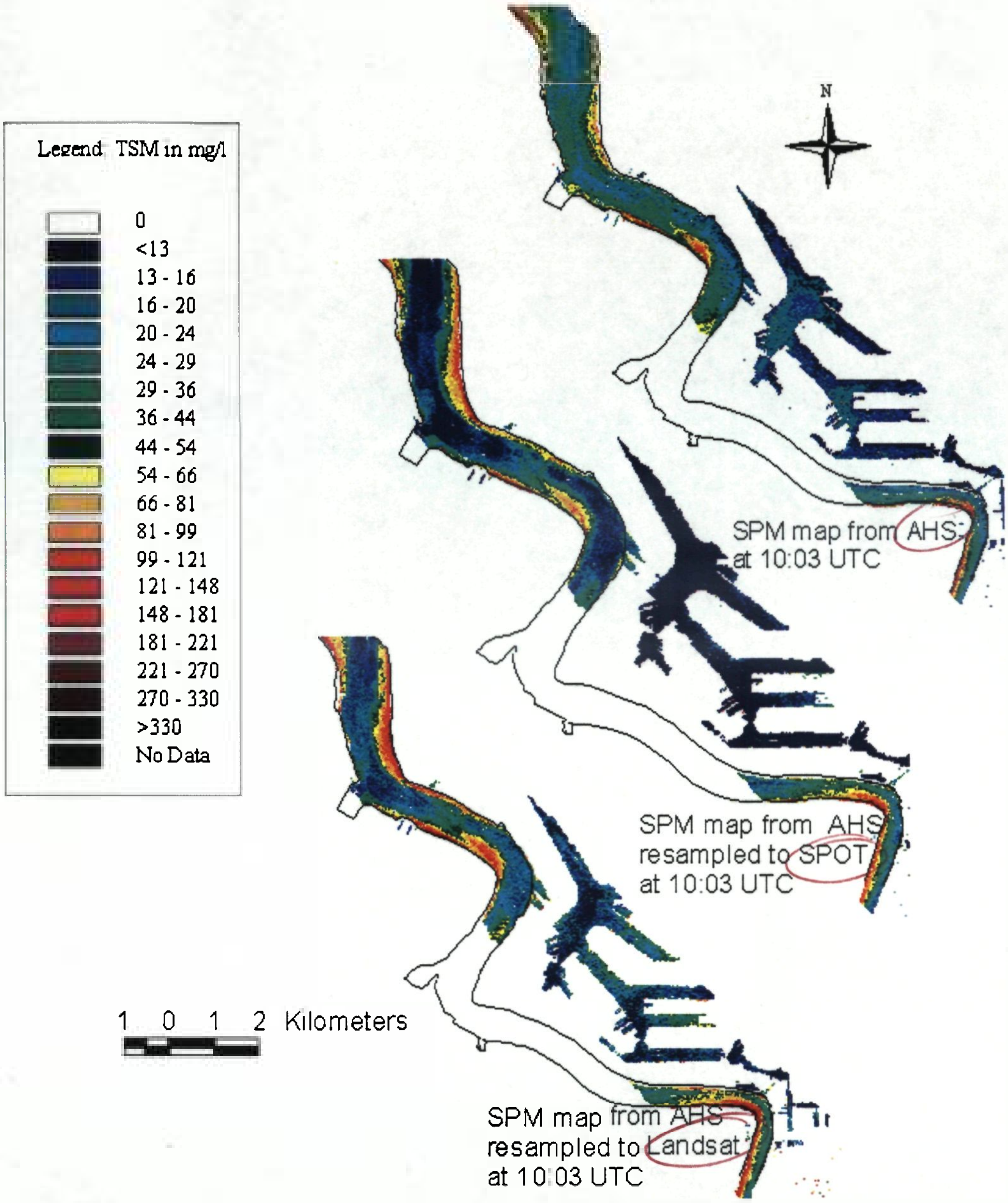

Figure 3 : Comparison of SPM maps derived from AHS data and AHS data spectrally and spatially resampled to SPOT and Landsat

ANNEX 7 - KOSTEFFICIENTIE VAN REMOTE SENSING VOOR ZWEVENDE STOF KARTERING

a. Remote sensing

4 types van kosten moeten in rekening worden gebracht :

1. set-up kosten
2. kosten voor de acquisitie van de remote sensing data
3. veldwerkkosten
4. kosten voor verwerking veldgegevens en remote sensing data

1. Set-up kosten

Onder set-up kosten verstaan we de kosten van de software en hardware die moeten aangekocht worden voor de uitvoering van de beeldverwerking. In tabel 1 wordt hiervoor een benaderende kostprijs gegeven. Deze aankoop moet maar éénmalig gebeuren zodat bij herhaaldelijk gebruik van remote sensing beelden de kost hiervan relatief laag is in vergelijking met de andere kosten. De gebruiker kan ook opteren om de geometrische en/of atmosferische correctie te laten uitvoeren door een onderaannemer of door de leveranciers van de vlieg- en/of satellietbeelden.

Tabel 1: Benaderende kostprijs set-up

SET-UP	Kostprijs (€)
Software	
Beeldverwerkingssoftware ENVI licentie	7 000*
Atmosferische correctie software ATCOR licentie	3 200*
Geometrische correctie software PARGE licentie	5 100*
totaal	15 300

*Andere prijzen gelden voor onderzoeksinstellingen en studenten.

In het kader van het ORMES project wordt er een softwarepakket ontwikkeld dat de nodige tools omvat voor het afleiden van zwevende stof kaarten uit atmosferisch en geometrisch gecorrigeerde beelden. IMDC hoeft daarom niet te investeren in een licentie voor een extra beeldverwerkingsoftwarepakket.

? exclusieve IMDC licence, of ook beschikbaar voor de markt?

2. Kosten voor de acquisitie van de remote sensing data

Hierbij moeten we in de eerste plaats een onderscheid maken tussen de aankoop van satelliet- en vliegtuigopnames. Satellietbeelden hebben een significant lagere kostprijs. Naast dit belangrijk voordeel hebben satellietbeelden ook niet te verwaarloosbare nadelen zoals:

- geen inspraak in het tijdstip van opname
- een lage temporele resolutie i.e. maximaal 1 per dag opname mogelijk (indien zelfde kijkhoek vereist is, is de temporele resolutie nog lager zie eveneens tabel 2)
- minder en bredere spectrale banden waardoor de fout op het geschatte zwevend stofgehalte vergroot (zie onderzoeksresultaten ......)
- geen data bij bewolking

Met satellietbeelden is het dus onmogelijk om de zwevende stofconcentraties over één getijde-cyclus in kaart te brengen. Het is dus aan de gebruiker om een kosten-batenanalyse uit te voeren.

In tabel 2 wordt de kostprijs gegeven voor de aankoop van de meest courante satellietbeelden met medium resolutie (20 – 100 m).

Tabel 2: Kenmerken (kostprijs, resolutie) van een aantal medium resolutie beelden

Type satellietbeeld	Kostprijs[1]	Spectrale banden	Temporele resolutie	Grootte beeld	Ruimtelijke resolutie
SPOT HRV SPOT (High Resolution Visible and Infrared)	nieuwe beelden : 2700 € archiefbeelden : 1900 € source : http://www.spotimage.fr/	Multispectraal : B1 0,50-0,59 µm B2 0,61-0,68 µm B3 0,79-0,89 µm MIR 1,58-1,75 µm Monospectraal : B2 0,61-0,68 µm	Absoluut : 26 dagen ² Andere hoek en satelliet[3] : +/- 1 dag	60 km x 60 km	20 m 20 m 20 m 20 m 10 m
ETM+ (LANDSAT-7) (Enhanced Thematic Mapper Plus)	600 $ (before 2003) 300 $ (after 2003)[4] http://landsat.usgs.gov/	B1 0,45-0,515 µm B2 0,52-0,605 µm B3 0,63-0,69 µm B4 0,75-0,90 µm B5 1,55-1,75 µm B 6 10,4-12,5 µm B7 2,09-2,35 µm PAN 0,50-0,90 µm	16 dagen ²	183 km x 170 km	30 m 30 m 30 m 30 m 30 m 60 m 30 m 15 m
ASTER	150 $ http://edc.usgs.gov/	VNIR 4 bands SWIR 6 bands TIR 5 bands	16 dagen ²	60 km x 60 km	15 m 30 m 90 m
ALI (Advanced Land Imager)	1000 $ http://edc.usgs.gov/	Pan 0.48 - 0.69µm B1' 0.43- 0.45 µm B1 0.45 - 0.51 µm B2 0.52 - 0.60 µm B3 0.63 - 0.69 µm B4 0.77 - 0.80 µm B4' 0.84 - 0.89 µm B5' 1.2 - 1.3 µm B5 1.55 - 1.75 µm B7 2.08 - 2.35 µm	16 dagen ²	37 km x 42 km	10 m 30 m 30 m 30 m 30 m 30 m 30 m 30 m 30 m 30 m
IRS LISS	2700 € http://www.euromap.de/	B1 0,52 -0,59 µm B2 0.62-0,68 µm B3 0,77-0,78 µm	24 dagen ²	148 km x 148 km	22.5 m 22.5 m 22.5 m
Hyperion	1000 $ http://edc.usgs.gov	220 banden	16 dagen²	7,7 km x 42 km	30 m

[1] Exclusief atmosferische en geometrische correctie ; dit zijn enkel richtprijzen, andere prijzen kunnen gelden voor studenten, onderzoeksinstellingen, archiefbeelden,….

[2] De absolute temporele resolutie is de tijdsperiode tussen 2 beeldopnames gemaakt door dezelfde sensor van exact hetzelfde gebied met exact dezelfde kijkhoek. Echter omwille van het feit dat er meestal een zekere overlap is tussen beelden van naburige satellietbanen, kunnen er wel meer frequent beelden worden genomen van de meeste gebieden maar dan onder een andere kijkhoek. De overlap tussen naburige satellietbanen vergroot bij grotere latitudes en dus de tijd tussen 2 heropnames vermindert.

[3]de temporele resolutie kan verhoogd worden door gebruik te maken van meerdere SPOT satellieten. De SPOT constellatie bestaat uit 4 satellieten waarvan 3 nog in gebruik. Daarenboven kan SPOT onder een oblique kijkhoek beelden nemen. Dit laat toe om 95 % van het aardoppervlak minstens 1 keer per dag in beeld te brengen.

[4] sinds 2003 zijn er problemen met Landsat. Prijzen gelden voor de U.S.

Een offerte werd aangevraagd voor de acquisitie van hyperspectrale CASI 2 beelden met een resolutie van 1- 2 m over een studiegebied in België. De kostprijs werd geschat op £ 8000 (exclusief BTW) voor 1 site van 25 km^2. Deze kost omvat de transit naar de site, de opname van de beelden en de radiometrische correctie (zonder atmosferische en geometrische correctie). Men kan dit echter niet beschouwen als de gemiddelde prijs voor beeldacquisitie met een hyperspectrale vliegtuigsensor. Het is immers moeilijk een eenduidige kostprijs te geven voor beeldopnamen met een hyperspectrale vliegtuigsensor daar deze kostprijs immers bepaald wordt door meerdere factoren zoals :

- ligging studiegebied (voor afgelegen gebieden stijgt de kostprijs door de hoge mobilisatiekosten)
- grootte studiegebied (kostprijs per m^2 daalt bij grotere studiegebieden)
- ruimtelijke resolutie beelden (hoe hoger de resolutie (kleinere pixels), hoe meer beelden nodig om het gebied te bedekken, hoe hoger de kostprijs)
- vereiste flexibiliteit van de dataleverancier (hoe flexibeler de dataleverancier moet zijn, hoe hoger de kostprijs)
- type hyperspectrale sensor

Daarnaast raden we de gebruiker aan om meerdere offertes aan te vragen. De kostprijs kan aanzienlijk verschillen tussen de dataleveranciers.

3. Veldwerkkosten

De veldwerkkosten hebben betrekking op het verzamelen van een voldoend aantal waterstalen ter calibratie van de zwevende stof algoritmes. In het hoofdstuk “sampling” wordt een schatting gegeven van het vereist aantal waterstalen in functie van de verwachtte accuraatheid van de uiteindelijke zwevende stof kaarten.

De waterstalen kunnen genomen worden vanaf drijvende pontons of vanaf meetboten. De kost van het nemen van deze waterstalen kan opgesplitst worden in vaste en variabele kosten. De vaste kost behelst de aankoop van dGPS systemen indien nog niet beschikbaar. De variabele kosten kan men opsplitsen in enerzijds personeelskost en anderzijds de huurprijs van de meetboten.

De huurprijs van de meetboten wordt beïnvloed door :

- type meetboot (in dit geval volstaat in relatief simpele boot daar er geen grote meetinstrumenten aan boord moeten enkel GPS en staalflessen)
- afstand tot de haven
- afstand tussen de verschillende meetpunten
- locatie
- Bemanning (schipper, machinist, matrozen, surveyors)

4. Kosten voor verwerking van de veldgegevens en remote sensing data

De kosten voor de verwerking van de veldgegevens hebben betrekking op de bepaling van de zwevende stof concentraties uit de waterstalen. De kostprijs hiervan kan verschillen tussen de laboratoria. Als richtprijs kan men 17 € per staal nemen. Dus voor 40 stalen komt dit neer op een kostprijs van 680 €.

De tijd (en de daarmee samenhangende personeelskosten) vereist voor de verwerking van de remote sensing data is afhankelijk van :

- de ervaring van de gebruiker
- het aantal te verwerken beelden
- processor snelheid van de computer waarop de beeldverwerking gebeurt

De bestaande beeldverwerkingssoftwarepakketten vereisen toch een zekere ervaring van de gebruiker vooraleer er vlot mee gewerkt kan worden. Er wordt verwacht dat met behulp van het softwarepakket dat binnen ORMES ontwikkeld wordt, de vereiste verwerkingstijd voor een zogenaamde "leek" in beeldverwerking kan geminimaliseerd worden. Dit kan doordat dit pakket specifiek zal ontwikkeld worden voor het karteren van het zwevend stofgehalte met behulp van remote sensing data.

De tijd vereist voor de preprocessing (geometrische en atmosferische correctie) werd hierbij niet in rekening gebracht daar we ervan uitgaan dat de beelden ofwel volledig gecorrigeerd worden aangekocht ofwel de preprocessing wordt uitbesteed aan een onderaanneming. De prijs voor preprocessing is sterk afhankelijk van het aantal beelden, type beeld en de leverancier.

b. Traditionele campagnes

1. set-up (mobilisatie en installatie) kosten
2. kosten voor de acquisitie van de data
3. demobilisatie
4. kosten voor verwerking veldgegevens

Deze prijzen zijn gebaseerd op een dertien-uursmeetcampagne, waarbij er gedurende de gehele meetperiode turbiditeitsgegevens (profielen) worden ingezameld met 1 turbiditeitsmeter (OBS3A) aan boord van 1 schip. Dit is inclusief een dGPS die meestal standaard aan boord van meetschepen aanwezig is en echosounder ter bepaling van de bodemdiepte. Er worden 30-40 waterstalen genomen ter calibratie van de turbiditeitsmeter. Deze worden geanalyseerd voor het bepalen van het zwevende stoffen gehalte conform Nederlandse norm NEN 6484. De verwerking van de data wordt gerapporteerd in een factual data report met verwerkte turbiditeiten.

Actie	*Prijs (euro excl BTW)*
Mobilisatie schip, installatie apparatuur	8500
Uitvoering 13-uursmeting	8000
Demobilisatie schip	3000
Verwerking, staalname-analyse en genereren rapport	4000
TOTAAL	**23000**

Vergelijking

Aankoop Satellietbeelden — SPOT 1300 € (archief); Landsat 600 € (archief)

Uitvoering meting + schip + peilen — 5000 €

Verwerking, staal=analyse + factual data report — 4000 €

Verwerking beelden — 2000 €

11 600 € — 12 300 €

TSM kaart op basis van satellietgegevens

ANNEX 8: VALIDATION USING TANSECTS

Extra validation is performed using a series of turbidity measurements at distinct points along horizontal cross-section transects made by IMDC in the past at different stages of the tidal cycle. The location of these transects is given in figure 1. As these measurements were not done coincident with the airborne data acquisition no absolute comparison of TSM concentration is possible. However these measurements can be used to verify observed patterns of TSM concentration change in function of the tide. In figure 2 TSM concentration in function of the tide derived from both the turbidity (left) and airborne data (15/06/2006, right) are given for all the transects. The time indicated on the x-axis is not the real time of measurement but it equals the time after high tide. In general the TSM patterns observed during the field measurements and derived from airborne data agree quite good. The 'Oosterweel left' transect shows relatively high TSM concentrations around high water, a strong decrease in the succeeding slack water and a gradual increase during ebb. For 'Oosterweel right' and 'Ka' similar patterns are observed. For the other transects these patterns are less consistent. For example, the SS concentrations at Oosterweel middle are relatively high at high water and low at slack water, during ebb both the transects indicate first an increase in TSM immediately followed by a decrease.

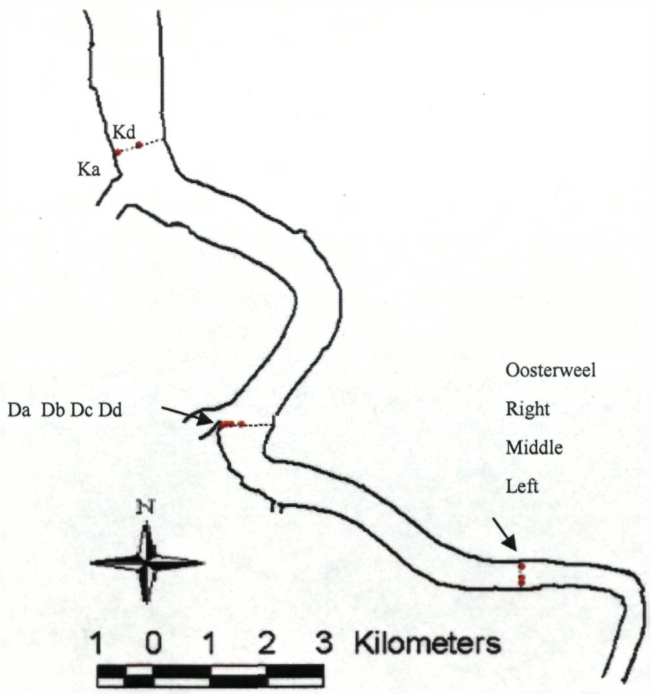

Fig. 1: Location of transects where turbidity measurements were performed in the past (transect 'Ka-d' 17 Feb. 2005; transect 'Da-b-c-d' 18 Feb. 2005 ; 'Oosterweel Right-Middle-Left' 3 June 2004 and 10 June 2004)

HCBS Ka 17/02/2005

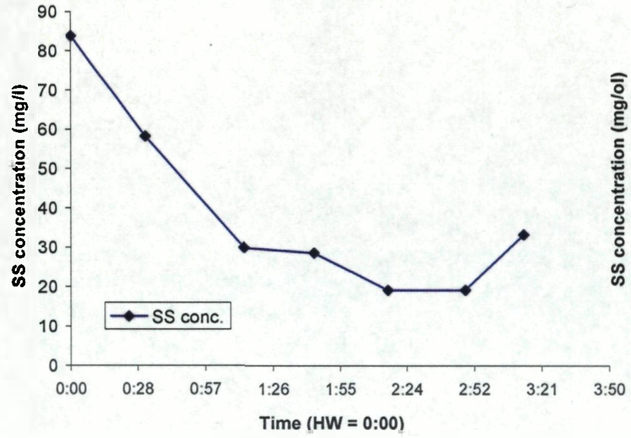

HCBS Ka 15/06/2005

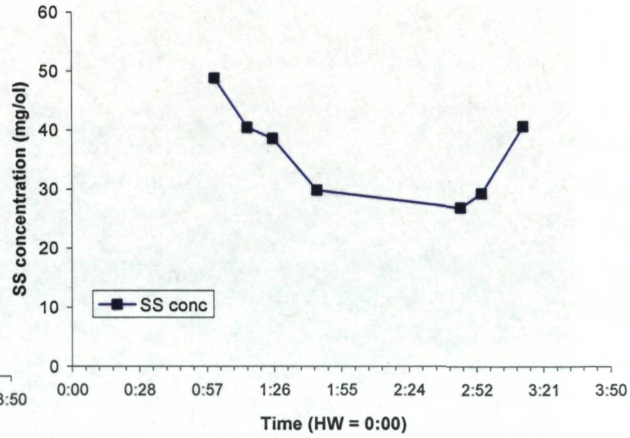

HCBS Kd 17/02/2005

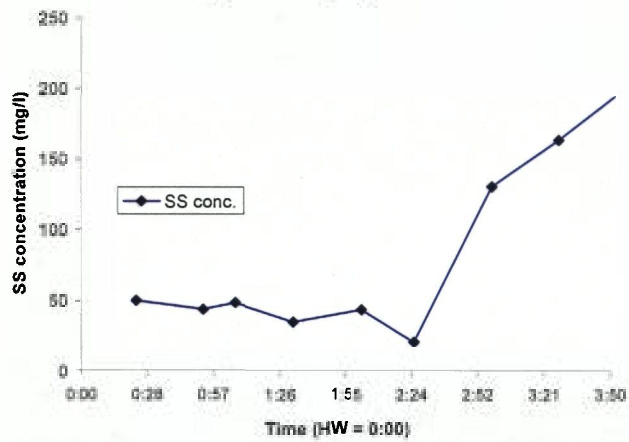

HCBS Kd 15/06/2005

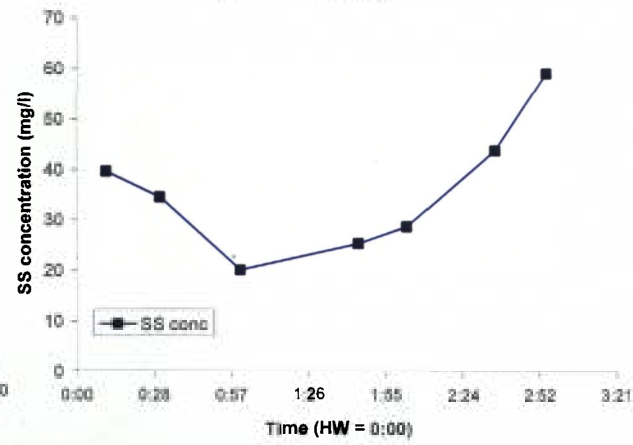

HCBS Da 18/02/2005

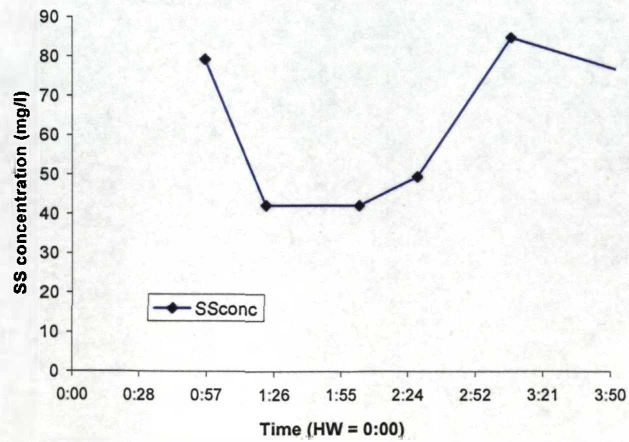

HCBS Da 15/06/2005

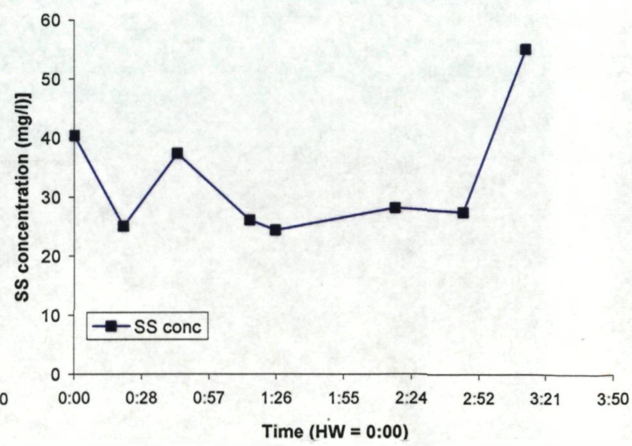

HCBS Db 18/02/2005

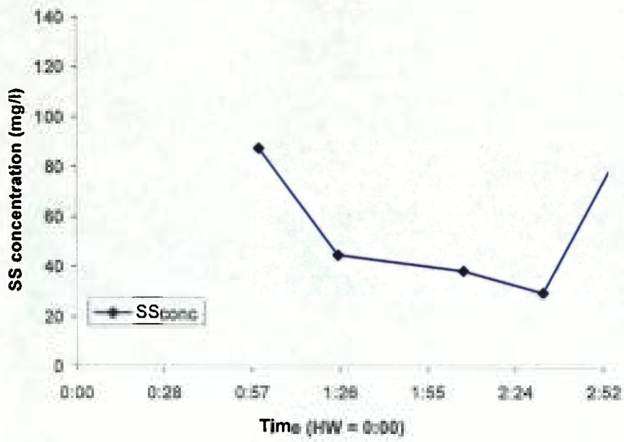

HCBS Db 15/06/2005

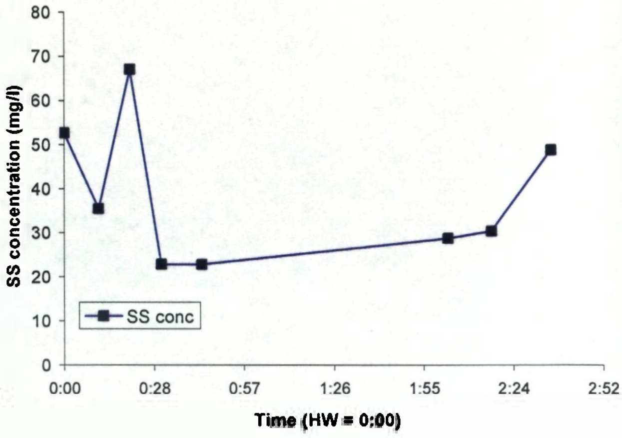

HCBS Dc 18/02/2005

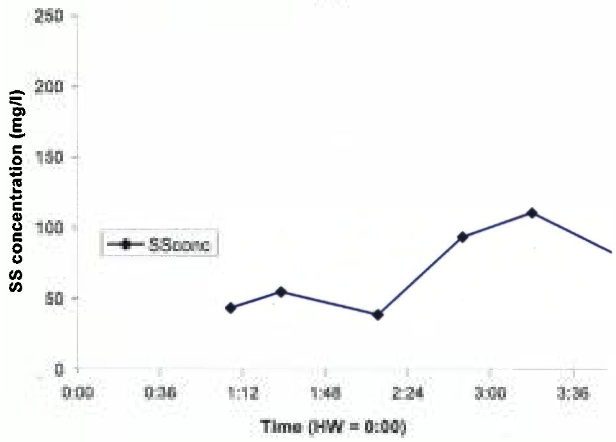

HCBS Dc 15/06/2005

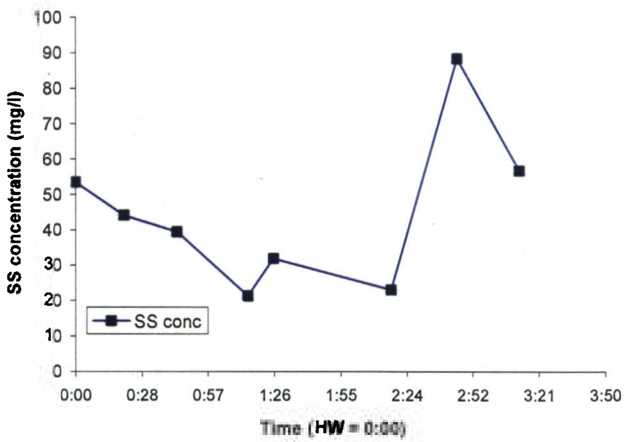

HCBS Dd 18/02/2005

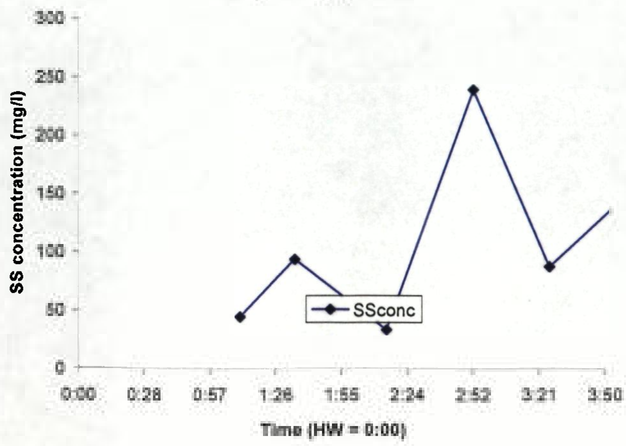

HCBS Dd 15/06/2005

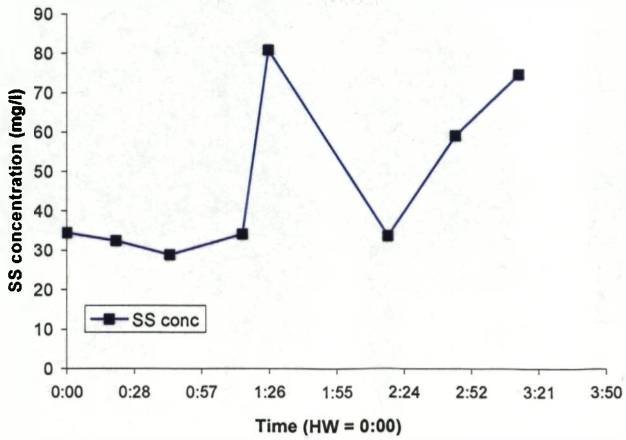

Meting

Remote Sensing

Oosterweel Left 03/06/04

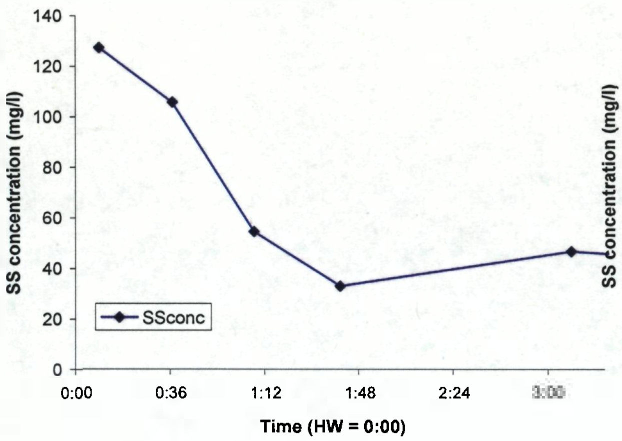

Oosterweel_left 15/06/2005

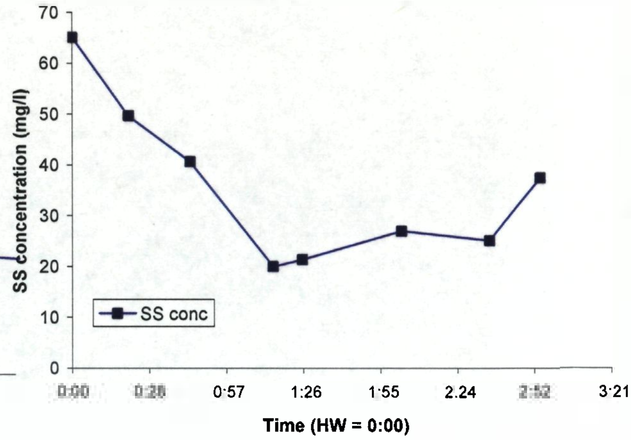

Oosterweel Left 10/06/04

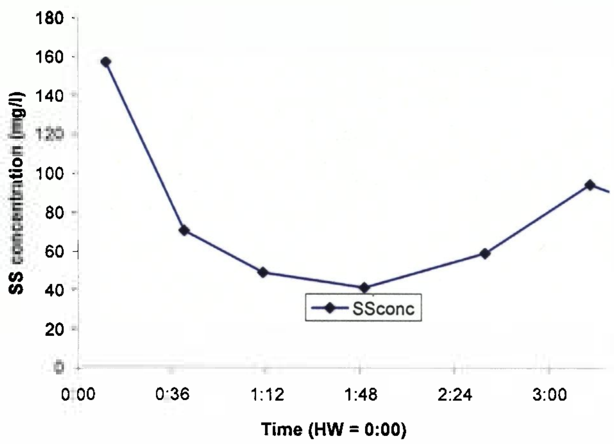

Oosterweel Middle 03/06/04

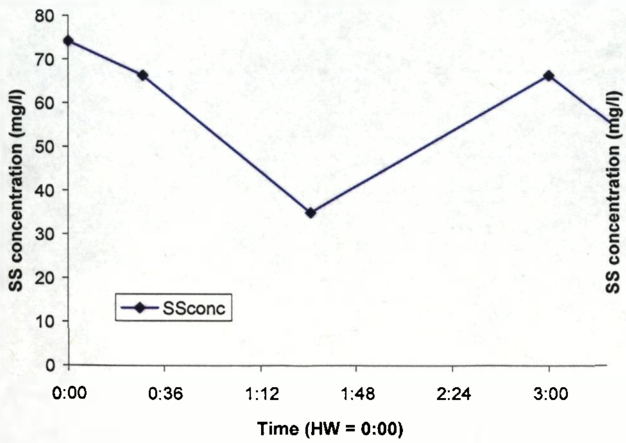

Oosterweel_middle 15/06/2005

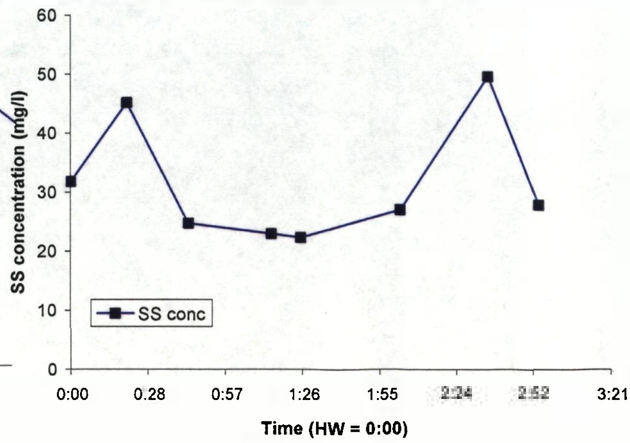

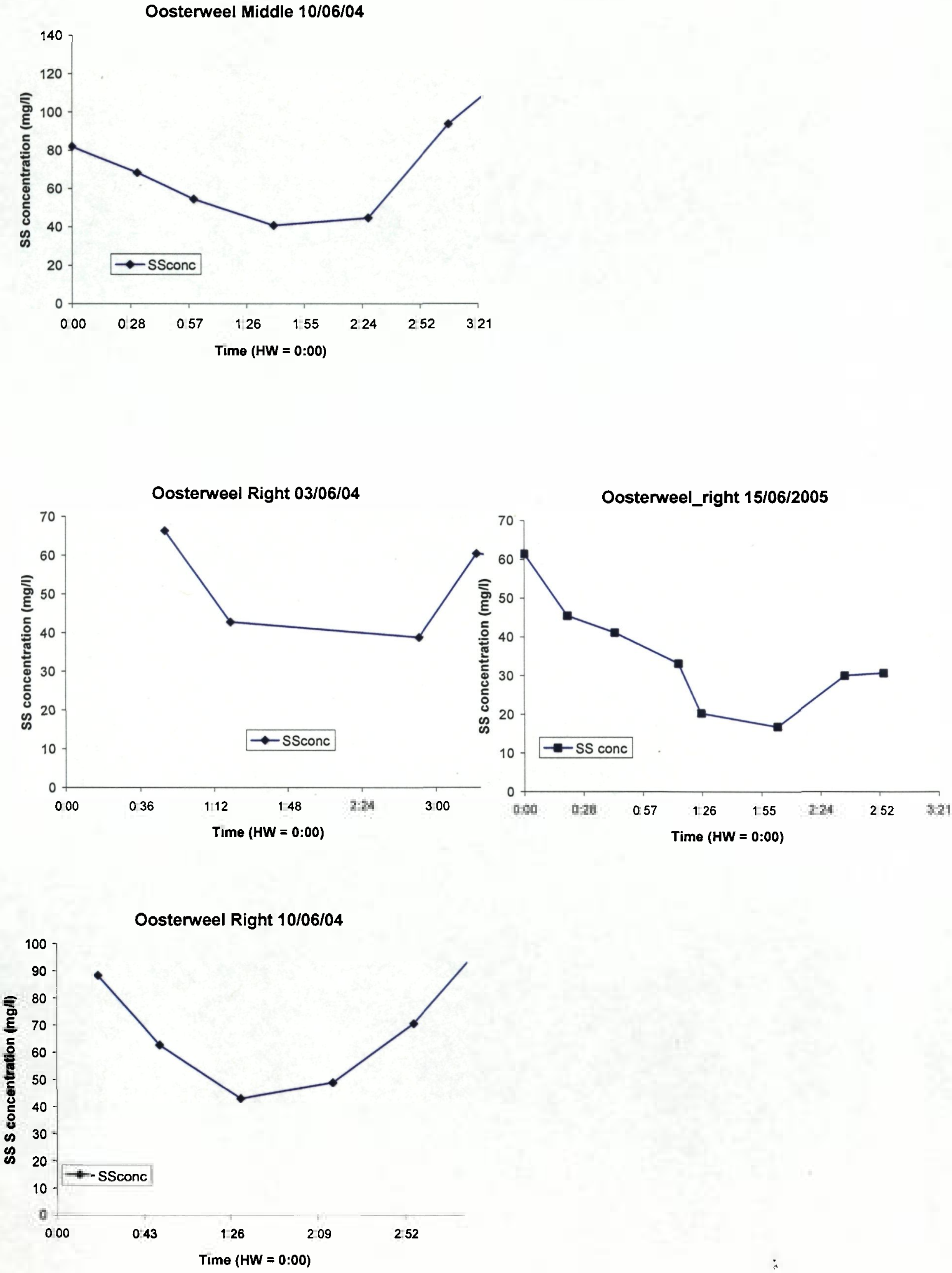

Fig. 2: Transects Ka , Kd, Da, Db, Dc, Dd, Oosterweel Left, Middle and right. field data are shown at the left and SS concentration derived from airborne data at the right